DEVELOPMENT OF A PLANAR TWO-PHASE COUNTERCURRENT SHEAR LAYER FACILITY

A THESIS

SUBMITTED TO THE FACULTY OF THE

UNIVERSITY OF MINNESOTA DULUTH

BY

UPOM LOUISE COSTA

IN PARTIAL FUFULLMENT OF THE REQUIREMENTS

FOR THE DEGREE OF

MASTER OF SCIENCE

DR. ALISON HOXIE

ADVISOR

JUNE 2023

Acknowledgement

I would like to thank my advisor, Dr. Alison Behrens Hoxie, Associate Professor at the Department of Mechanical Engineering, University of Minnesota Duluth for her continuous support and motivation throughout my Master's. She has been a kind and patient mentor helping me with research and my personal and academic life.

I would also like to thank my family members for their unconditional love and support throughout my life. Without them this achievement would not have been possible. Special mention goes to my mother who has always been guiding and motivating me. Her hard work and dedication is something I dream to achieve one day.

Lastly, I thank Zachariah Coughlin whose contribution in this project has to be mentioned. He helped me starting from the initial days of the project until the last days before I wrapped up my work. I also thank Caleb Heidelberger and Jordan Gruenes who were also supportive and helped me for various things.

Dedication

I dedicate my work to my mother, who has helped me reach where I am today.

Abstract

Efficient atomization of viscous liquids has widespread applications in industry. Numerous research articles have focused on trying to make the atomization process more efficient and less energy consuming. While conventional atomizers have struggled with the efficiency of the atomization of highly viscous liquids, a counterflowing nozzle recently developed at the University of Minnesota have shown remarkable results in spraying liquids ranging in viscosity from 54 cP to over 1000 cP and producing sauter mean diameters of less than 50 microns at Air to Liquid Ratios ranging from 0.1 to 0.5. Upon closer investigation, it is assumed that extremely thin shear layers might be formed on liquid and air streams leading to interfacial instabilities of very short wavelength. The work here aimed at designing and building an experimental facility to test the dynamics and spatiotemporal evolution of interfacial instabilities a planar two-phase countercurrent mixing layer. The facility has the unique features of facilitating both fully closed and partially open channel experiments. The movement of the secondary jet allows to study the spatial development of the shear layer. As initial tests in this new facility, water-water single phase countercurrent shear layers were set up. High speed back illuminated camera and a mobile camera array recorded the interactions between the primary and the dye-injected secondary stream. Three different flow rates were observed which provided different flow characteristics. The secondary flow rate was varied between 3 to 12 gpm keeping the primary stream velocity constant. Qualitative analysis was performed by comparing the streamwise and spanwise flow structure development for all cases.

Table of Contents

List of Tables

List of Figures

1. Introduction

A wide variety of industries have to deal with mixing in two-phase flows for creation of emulsions and suspensions by mixing liquid and gas streams at fine scales to produce finer droplets, e.g., cosmetics, pharmaceuticals, chemical reactors, food processing, petroleum, agriculture, etc. (Figure 1). Atomization of bulk liquid - "the process of a liquid jet or sheet disintegrating by the kinetic energy of the liquid itself or by exposure to high velocity air or gas," [1] occurs in liquid fuel combustion, spray painting in buildings and automobiles, spray drying of food products, spray coatings in textile and pharmaceutical, pesticide application. This process becomes very energy intensive when it comes to atomizing viscous liquids. Because of this, the higher viscosity of the more bio-friendly renewable jet fuels (>25 cP) becomes a deterrent when it comes to transitioning away from fossil fuels (<10 cP) since it prevents the formation of finer droplets which is essential for clean combustion.

Figure 1 - Use of atomization to produce finer sprays in automotive and agriculture industry

Figure 2 provides the schematic of an internal mixing counterflow nozzle that was developed at the UMN. This nozzle has been shown to be very energy efficient requiring only half to one-third amount of the air required for other commercially available nozzles [2]. While spraying water (1 cP), the nozzle was able to produce small droplet diameters with a tight distribution ratio using only half the mass air flowrate, which translates into 50% reduction in energy at constant inlet pressure (Figure 3). In addition, it was able to atomize highly viscous liquids like Propylene Glycol (54 cP) and 85% Glycerol (134 cP) at very low mass flow ratios (less than 0.25) and produce sauter mean diameters of less than 50 microns. The mechanism at work here differs from other internal mixing designs such as effervescent [3] or flow blurring [4] atomizers. Upon close investigation, the mechanism related to this efficient atomization is still to be determined. High-fidelity simulations revealed that inside the nozzle, Kelvin-Helmholz type of instability of the liquid jet was contributing to spray formation which essentially made it insensitive to the viscosity of the liquid [5]. After observing the flow visualization results, it is evident that the flow appears to emerge from the nozzle orifice directly as droplets instead of a liquid jet that undergoes primary and secondary atomization. In comparison to a flow-blurring nozzle, it produces smaller droplet diameters and is capable of atomizing much more

viscous liquids. It is predicted that extremely thin shear layers might be formed on liquid and air streams leading to interfacial instabilities of very short wavelength [2]. However, further studies need to be conducted to confirm this.

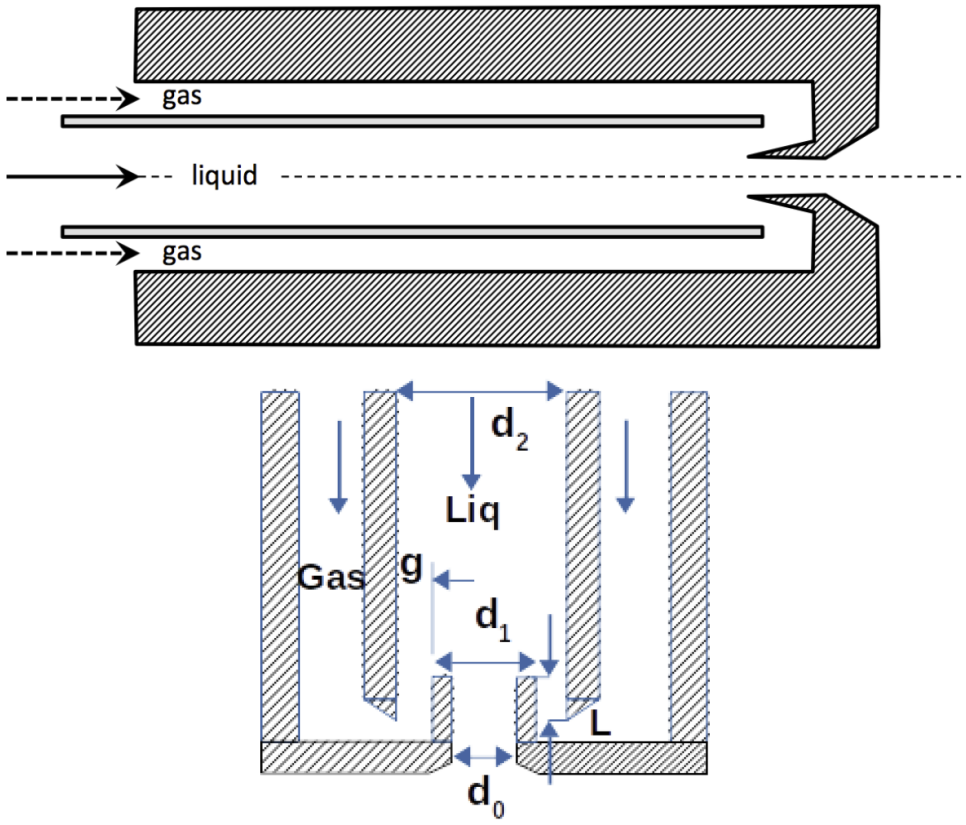

Figure 2 - Schematic Diagram and cross section of the counterflow nozzle exit showing the fluid directions (a) and the internal geometry (b) [2]

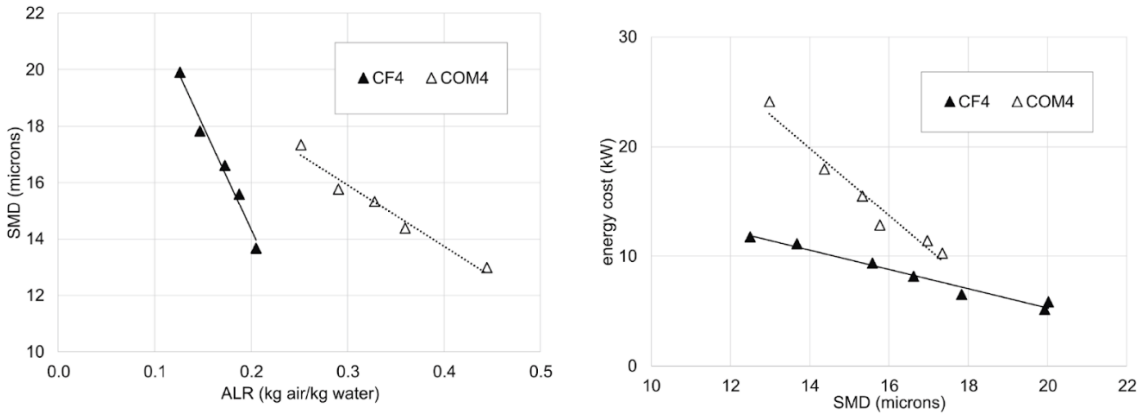

Figure 3 - Results comparison at water flow of 4.2 g/s (a) Counterflowing nozzle (CF4) requires half the air in comparison to a commercial nozzle (COM4) to produce similar SMD, (b) At constant inlet pressure which means almost 50% reduction in energy cost [2]

While researchers have been focusing on counterflowing shear layers for the last few decades, most of the literature have been single phase studies. [6][7][8] Attempts of establishing momentum-driven countercurrent flows were unsuccessful because of flow stagnation and instability. [8][9] Consequently, alternative options like using suction driven facilities were employed [10] [11] [12] until Anderson [13] developed a momentum driven facility to study counterflowing shear layer between two air streams. However, the facility is limited to studying single phase counterflowing air streams. To determine the mechanism inside the counterflowing nozzle, a momentum driven a two-phase countercurrent shear flow facility is required to further advance the understanding of counterflowing shear layers. As of today, such facility does not exist and these studies have not been performed yet.

As a result, in this study, a facility is designed and built with the goal in mind to explore and analyze the mixing characteristics and the length scales in a planar two-phase countercurrent shear layer in relation to the breakup mechanisms responsible for liquid atomization. This facility has the unique capability to study countercurrent shear layer in partially and fully confined set up. After assembling the complete experimental set up, single phase counterflowing water shear layers are studied here first with the help of high-speed imaging and a mobile phone camera array. During the study, three cases were studied by varying the secondary flow rate from 3 to 12 gpm and the effects of changing the momentum ratio on the flow interactions were recorded. The primary flow rate was kept constant for all the cases. Qualitative analysis was performed by comparing the streamwise and spanwise flow structure development for all cases. Subsequently, studying multiphase water-air shear layers are explored and future studies are recommended.

Section 2 tries to provide a brief review of all the necessary and relevant terminologies for the readers while section 3 provides an in-depth overview of all the previous works in countercurrent shear layers and multiphase coflowing shear layers. Methodologies are explained in section 4. Results are described in section 5 of the text. The findings are concluded and future work is discussed in section 6.

2. Background

2.1. Shear Layer Definition

A ***shear layer*** is defined as the mixing region containing a velocity gradient that is formed between two quasi-parallel fluids that are at somewhat different conditions, thus sometimes also called the ***mixing layer*** or ***vorticity layer***. A ***boundary layer*** is a form of shear layer where momentum transport is affected by a solid interface causing the viscous forces to dominate only until a certain distance, unlike free shear flows (Figure 4). In many texts, all four of these are used interchangeably. The mixing between the two streams is contained in the region of the shear layer. Depending on the direction of the fluid streams, the shear layers can either

be coflowing or counterflowing. A ***coflowing shear layer*** (Figure 5a) occurs when the secondary stream is in the same direction as the primary flow. A ***counterflowing or countercurrent shear layer*** (Figure 5b), on the other hand, is seen when the secondary fluid is flowing opposite to the primary fluid stream. Coflowing shear layers can be found in various mixing processes and aviation applications while counterflowing shear layers are seen most prominently in cases of flow separation.

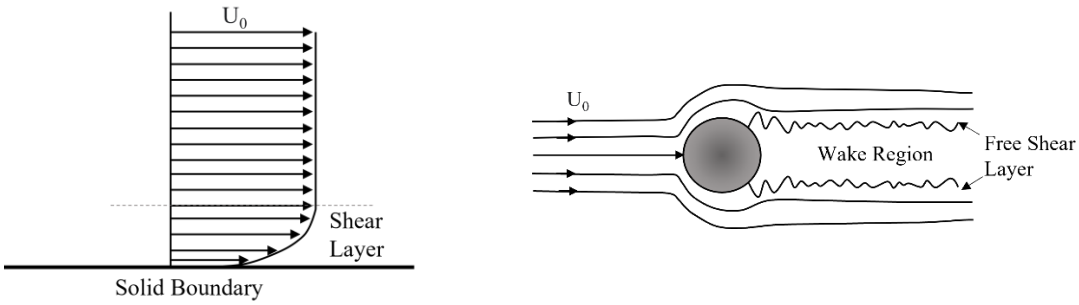

Figure 4 - Boundary Layer and Free Shear Layer

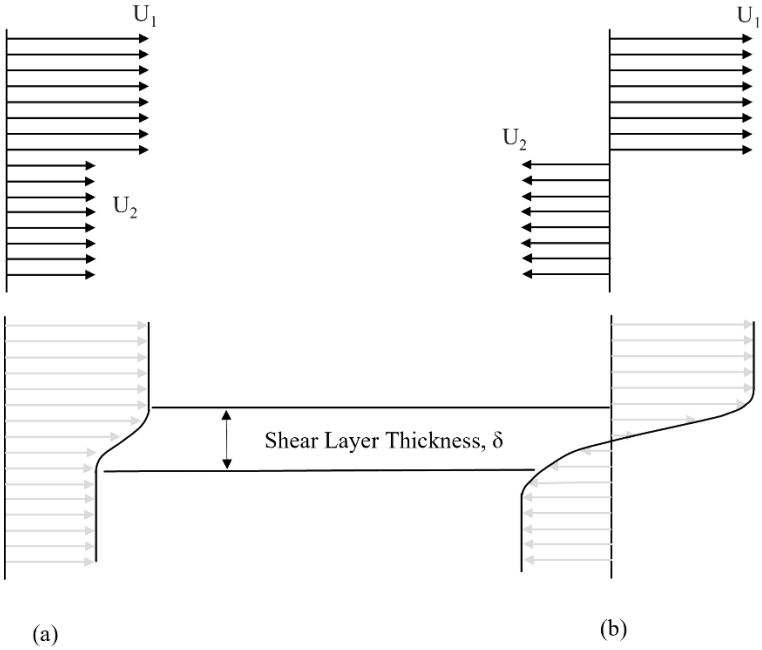

Figure 5 - (a) Coflowing Shear Layer (0<λ<1); (b) Counterflowing Shear Layer (λ>1); For free shear layers, U_2=0, λ=1

While the shear layer profiles may vary based on a few important parameters like velocity, density, temperature, etc.; shear layer thickness (δ) and growth rate (ω_i) have been the two most focused parameters among the researchers [6,7]. Different measurements of shear layer thickness are available:

Vorticity Thickness, $\delta_\omega = \frac{U_1 - U_2}{(\frac{\partial u}{\partial y})_{max}}$

where, U_1 and U_2 are the fluid velocities in the primary and secondary sides respectively; the denominator term represents maximum cross-stream mean velocity gradient.

Velocity Thickness, $\delta_v = y_{95} - y_5$

where, y_{95} is the location where the velocity is $u = U_2 + 0.95(U_1 - U_2)$ and y_5 is where $u = U_2 + 0.05(U_1 - U_2)$, u is a function of location in x and y and is the local mean velocity component in the streamwise direction.

Another two primary parameters are the velocity ratio and the normalized velocity ratio. The velocity ratio (r) is defined as:

$$r = \frac{U_2}{U_1}$$

and the normalized velocity ratio parameter (λ) is defined as:

$$\lambda = \frac{U_1 - U_2}{U_1 + U_2}$$

where, U_1 is the primary flow velocity and U_2 is the secondary flow velocity.

Shear layers may develop in time and or space. A shear layer developing in time is called a ***temporally developing shear layer***, which generally has a flow at uniform initial condition along the streamwise direction and the shear layer is established in time because of the shear applied to the flow (Figure 6a). Thorpe (1971) [6] studied a temporally developing shear layer in his tilting tank experiment. Temporally developing shear layers are helpful in analytical and computational studies. Another kind of shear layer is the ***spatially developing shear layer*** in which shear layer thickness is generally a function of the distance along the streamwise coordinate, meaning that shear layer growth depends only on distance (Figure 6b). This type of shear layer is created by splitter plates or other geometries inducing adverse pressure gradients. Most practical applications see this kind of shear layer, therefore more experimental studies have been conducted to study shear layers of this category. It is also possible to create shear layers that exhibit growth in both space and time. Previously, theoretical predictions have been made using spatiotemporal linear stability analysis for different cases. [14][15]

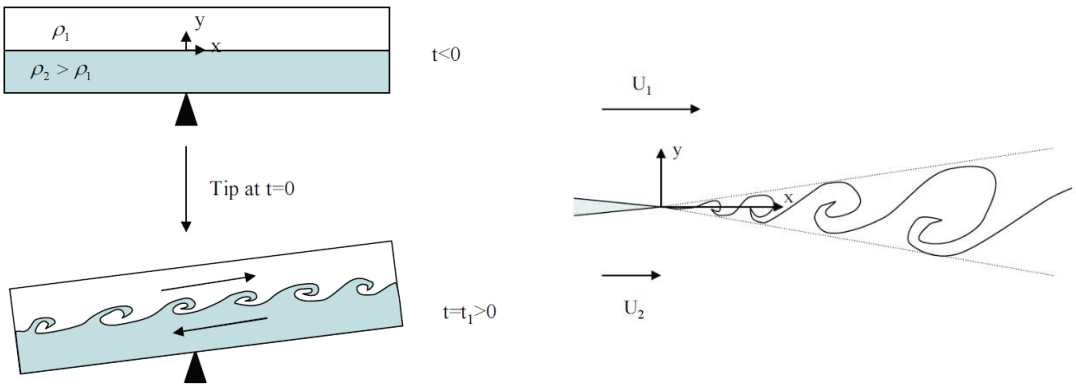

Figure 6 - (a) Temporally developing shear layer; (b) Spatially developing shear layer [9]

Just like boundary layers, the shear layers can be laminar or turbulent. A spatially developing shear layer grows downstream and becomes turbulent. Shear layers can be tripped too, to become turbulent. [10] As the two streams of fluid interact, the difference in momentum is diffused through viscosity and turbulent transport, which leads to shear stresses and formation of vortices. Turbulent shear layers, therefore, promote enhanced mixing characteristics and have been widely studied. [9] [10] [16]

2.2. Shear Layer Development

For a spatially developing shear layer, two distinct regions characterize the shear layer development: the developing region and the fully developed region (Figure 7). The ***developing region*** is where the flow is highly three-dimensional because of the organized initial vortex structures interacting with each other. This region is mostly dominated by amplification of the upstream disturbances while the dissipation mechanism becomes more crucial downstream. The vorticity remains the highest in this region causing the growth of the shear layer to be nonlinear. The scales present in the shear layer are smallest in this region but increase with downstream distance. Energy is transferred between these scales, from large to small vortices through vortex stretching. At the end of the developing region, the flow becomes independent of any upstream disturbances and is said to enter the ***fully developed region***, also known as the ***self-similar region***. In this region, the flow quantities (primary and secondary mean velocities, shear layer width, etc.) are only dependent upon local variables. Upon achieving self-similarity, mean and fluctuating statistics across the shear layer can be collapsed on a single curve when properly normalized against local variables. The rate of growth of the shear layer is linear in this region. [16], [17], [18] From the growth and location of the shear layer in this region, the "virtual origin of the shear layer" can be found. [Figure 7]

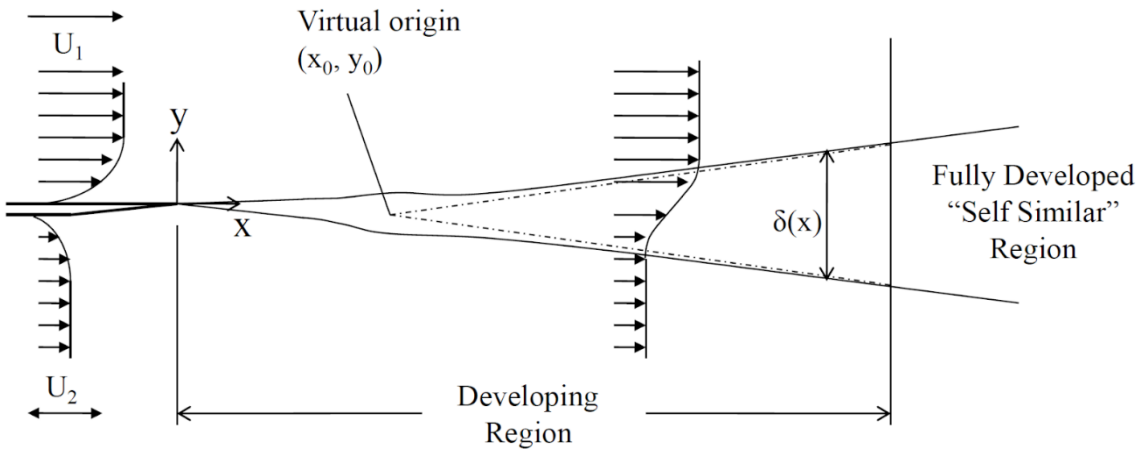

Figure 7 - Shear Layer Development [13]

2.3. Shear Layer Stability

There is a wide range of definitions of stability available based on different systems. A fluid mechanic system is said to be 'stable' if it can return to its original configuration after being imposed with infinitesimally small perturbations or disturbances that will die down with time. On the other hand, the system is 'unstable' if the smallest disturbances grow in amplitude and it fails to return to its initial state. Instabilities for a fluid flow can be different too based on the growth of the disturbances. A ***convective instability*** (Figure 8a) occurs when the disturbance grows but is also simultaneously moved away from the source, i.e., the quantity (such as velocity etc.) becomes unbounded with changing both time and position. Convectively unstable flows behave as amplifiers to external noises and give rise to wave packets that move away from the source and ultimately leave the medium in its undisturbed state. For ***absolute instability*** (Figure 8b), the disturbance starts to grow at the location of the source and subsequently spreads elsewhere, i.e., the quantity grows unbounded in time at a particular point and the flow gets contaminated everywhere by a point-source input. In other words, the system behaves as an oscillator [19]. For convectively unstable flows, the response of the system depends on the injected perturbations, whereas for absolutely unstable flows, the response of the system is independent of the injected perturbations. [20]

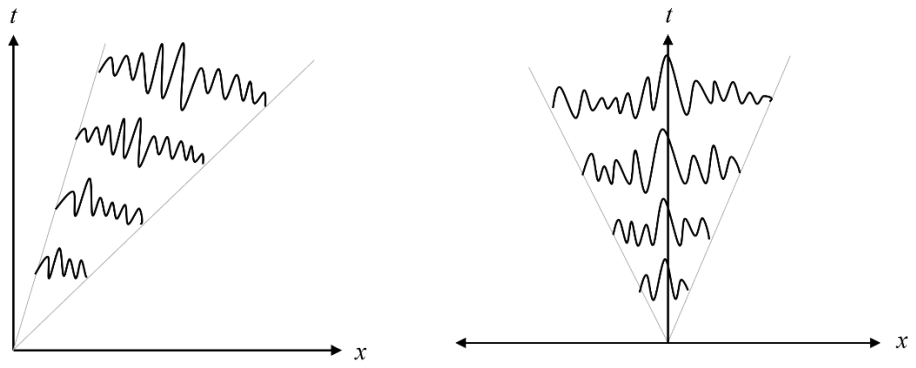

(a) (b)

Figure 8 - (a) Convectively unstable (b) Absolutely unstable

Since most shear flows are not uniform spatially, local and global concepts of stability might differ. Locally convectively unstable flows may be considered "globally stable" in the sense that they may lack self-sustained resonant modes (keep in mind that the flow is not actually hydrodynamically stable for all finite-amplitude perturbations). Local absolute instabilities, however, may exhibit self-excited global modes and therefore be considered "globally unstable." [19] In real-life scenarios, a major transition may occur from convective to absolute instability depending on changing critical control parameters. In dynamical systems, a ***bifurcation*** is said to occur when a sudden 'qualitative' change in the behavior of the system is induced by a small smooth change made to one of the parameters (bifurcation parameters). For the limiting value of the control parameter, shear flows exhibit a bifurcation point to global modes. For a more in-depth understanding of these concepts, see Huerre & Monkewitz (1990) [19].

Linear stability theory has been widely used analytically for spatiotemporal analysis and to predict the stability behavior of a system. In this theory, small perturbations are introduced mathematically to the set of governing flow equations, which are then linearized for subsequently solving and obtaining 'the dispersion relation' between frequency, ω and wave number, k. Numerically, a set of velocity, density, and viscosity profiles is said to be absolutely unstable if the dispersion relation for a wave packet displays a saddle point in the complex wave-number plane (k_i - k_r plane) with a positive absolute growth rate (imaginary part of the frequency, ω_i) that also corresponds to the amplification of upstream- and downstream-traveling waves (Figure 9).

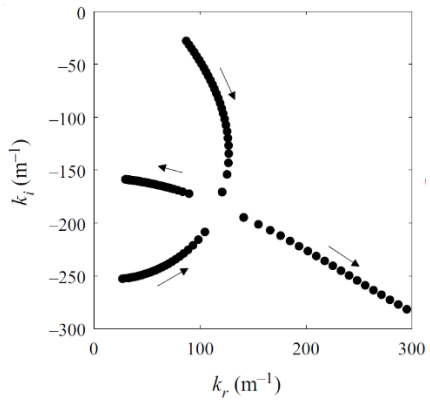

Figure 9 - A saddle point in the complex wave number plane with ω_i = 30 Hz demonstrating absolute instability [15]

3. Previous Work

There have been numerous studies on the dynamics of coflowing shear layers ([16], [21], [22], [23]) but counterflowing shear layers started receiving more attention in the past 30 years. This is primarily because of the difficulty of studying them in an experimental setup.

3.1. Counterflow Early Work

Thorpe (1968 & 1971) [6], [7] was the first to perform the tilting tank experiment by containing two stratified fluids initially in equilibrium and looked into a temporally developing countercurrent shear layer that has fluid dynamic features that are periodic in the streamwise coordinate by tipping the tank at a referenced time. The flow had a negative velocity ratio of r = -1 in the experiment, which showed the vortex roll-up process between the two streams, but the flow ultimately became unstable since the convective velocity, U_c was zero. Upon exploring the spatiotemporal stability of planar shear layers, Huerre and Monkewitz (1985) [24] showed analytically that the shear layer experiences a transition from convective to absolute instability beyond the counterflow velocity being 13% of the primary stream (r = -0.136, λ = 1.315) for a hyperbolic tangent velocity profile.

Establishing momentum-driven countercurrent flows has proved difficult because of global stagnation, flow reversal and unstable flow. Humphrey & Li (1981) [8], for example, tried to study a confined spatially evolving countercurrent shear layer consisting of two opposite momentum-driven streams separated by splitter plates. The goal was to examine the mixing between the two streams. However, a global stagnation zone was developed causing the flow to stagnate and turn 180° from the initial direction. Alvi et al. (1996) [9] developed a momentum-driven countercurrent shear layer using two opposite jets with no dead zone in between them, having a convective Mach number of M_c = 2 which resulted in zero convective velocity (U_c),

reporting enhanced mixing with no detail measurements. It was suggested that it might be caused by global instability.

As a consequence, suction driven facilities were used to study countercurrent flows experimentally for a long time ([10], [11], [12]). Strykowski and Niccum developed an axisymmetric facility by applying suction through an annulus around the jet to study the spatial development of the jet and analyzed the stability characteristics of the generated countercurrent shear layer by looking at the shear layer oscillations (1991) [25]. Later, they investigated the critical velocity ratio proposed by Huerre and Monkewitz (1985) [24] and the density ratio effects by Pavithran and Redekopp (1989) [26] Countercurrent shear was generated in a laminar round jet giving a critical velocity ratio in good agreement with the linear stability theory. When velocities approached $\lambda = 1.3$ for constant density, an abrupt transition was found which affected the overall mixing, matching the results from Huerre and Monkewitz (1985) [24]. As the density ratio increased, the critical velocity ratio for the convective to absolute instability also went up (1992) [27]. Khemakhem (1997) [28] was the first to attempt to study the planar countercurrent turbulent shear layer in a partially unconfined setup using a suction driven secondary flow. He was able to demonstrate some basic features of the shear layer without setting up a global stagnation like Humphrey & Li (1981) [8] but there were high uncertainties in the data because of experimental instruments.

Forliti et al. (2005) [10] also used a suction driven secondary stream and studied the spatial development of planar incompressible countercurrent shear layers experimentally by varying the velocity ratios (r) between 0 and -0.3 between two air streams ($\lambda = 1$ to 1.86) which to most extent agreed with analytical analysis. The shear layer growth rate increased with increasing counterflow and was found to be twice as large for 30% counterflow in comparison to the case with no counterflow or single free stream shear layer. A bifurcation in the flow field was found experimentally when the counterflow velocity ratio exceeds 13% of the primary stream ([11], [12]). Peak turbulence quantities, otherwise constant for low levels of counterflow, increased by up to 30% above 13% of the primary stream velocity which was kept constant at 31 m/s, as a result, this was also accompanied by mean three-dimensional flow. This was in agreement with the work of Huerre and Monkewitz (1985) [24].

Anderson (2011) [13] was the first one to develop momentum driven countercurrent shear flow with reliable measurements using two different facilities without setting up a global stagnation zone as before. He explored the options of using these partially confined facilities as control strategy in a dump combustor. His experiment included two opposing air streams, one at constant primary inlet velocity of 10.1 m/s while varying the secondary mass flow rate from 0% to 36% of the primary flow. The first setup was inspired by Alvi et al. (1996) [9] (Figure 10a) and the second setup used the Coanda effect to avoid the global stagnation observed by Humphrey & Li (1981) [8] (Figure 10b). The only difference between the facilities was that the second setup removed the secondary jet hardware to make room for the spatial growth of the shear layer by using the Coanda effect.

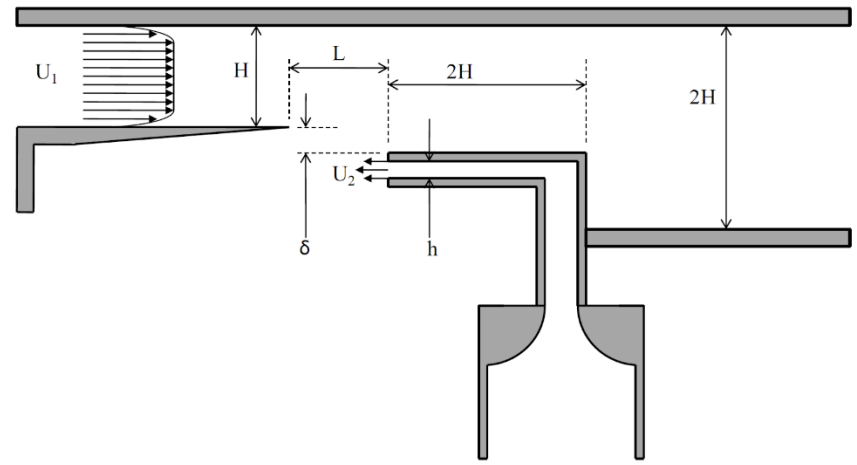

(a)

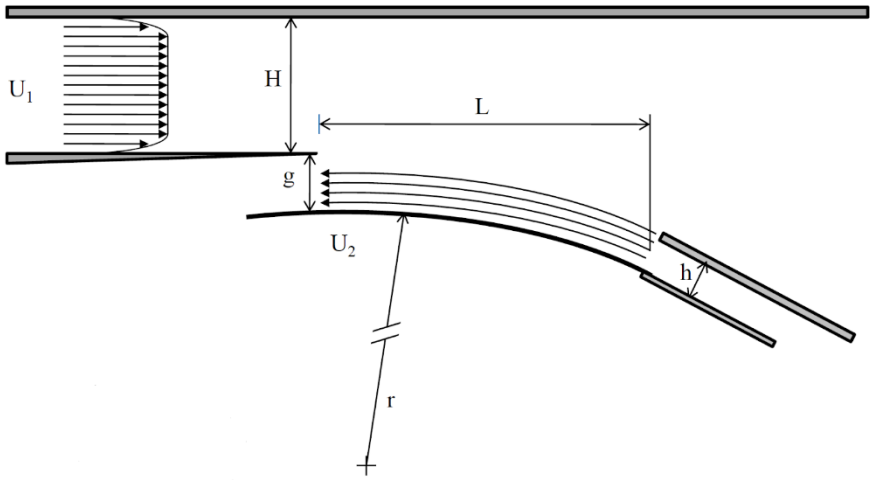

(b)

Figure 10 - The facilities used by Anderson (2011) to develop momentum driven counterflow [13]

The first setup (Figure 10a) was enclosed with walls downstream of the secondary jet, which was vertically kept 0.15H below the spitter plate where H is the height of the primary stream. During the study, four recirculation zones were found near the jet, primary and downstream recirculation zones being the predominant ones. With increasing secondary flow, the downstream recirculation zone got smaller while the primary recirculation zone increased in size. The streamwise, cross-stream, and total turbulence all grew with increasing secondary flow while having the largest turbulence near the secondary jet. It was found that the large turbulence levels reported were in fact not “turbulence” but flow disturbances due to the flopping motion of the secondary jet which was not consistent. As a result, this flow was regarded unacceptable as a control mechanism for creating stable anchor flame. Forcing studies revealed a global transition at 14% secondary mass flow rate which translates into the primary recirculation zone having 30% reverse flows in

comparison to the primary flow which matches the criteria described by Hammond and Redekopp (1998) [29].

On the second facility (Figure 10b), because of the curved surface, the flow remained attached through the Coanda effect which fixed the secondary jet location and, as a result, eliminated the flopping. Unlike the first one, this facility was open downstream of the secondary jet. Three gap sizes were tested with vertical gap heights of 8, 6 and 4 mm. It was found that the largest one (8 mm) set up a 'dead zone' with zero velocity and the smallest one (4 mm) created a global stagnation point similar to Humphrey & Li (1981) [8]. So, all experiments were carried out at 6mm, g/H = 0.3 which gave a smooth shear layer profile. Similar to the closed facility, increasing secondary flow rate caused an overall increase in the turbulence components indicating increased mixing within the shear layer. This also produced lower convective velocity of the countercurrent shear layer, U_c causing rapid shear layer growth. The facility showed very slight sidewall effects along with some three-dimensional flow at higher flow rates when undisturbed. Forcing studies show that spectral distributions in this flow field are spectrally broad, dominant peaks are not that apparent, and a transition is not seen as before. After forcing, the flow became highly three-dimensional over the entire domain, even at low secondary mass flow rates because of an assumed global transition in stability at 5% mass flow rate which corresponds to 30% reverse velocity. It was suggested that the stability, in this case, might be determined by Falker-Skan type of profiles of a wall-bounded recirculation bubble rather than tanh profiles of a planar countercurrent shear layer. The geometry was limited by it's inability to keep the secondary jet attached at lower velocity ratios under forcing study. However, the facility showed great promise as a control in combustion applications.

3.2. Multiphase Studies

All the works discussed until now have been single phase, mostly air-air systems. Although study of momentum-driven countercurrent water-air systems have not been reported by anyone, a huge body of work has been done on multiphase water-air coflowing shear layers. [30] [31][32][33] The following papers have been studying the destabilization of a slower moving water jet via an adjacent faster coflowing air jet which possess some similarities to the study conducted here. However, in all these cases, the high velocity air stream was the primary side and the low velocity water stream was considered the secondary side.

Marmottant and Villermaux (2004) [34] studied both experimentally and analytically the instabilities associated with the atomization steps of a slowly moving axisymmetric liquid jet by a coaxial fast-moving gas stream. During the study, they obtained a scaling law between the frequency and the gas velocity, $f \sim {U_g}^{3/2}$ which agreed relatively well with Matas et. al (2011) [35], Raynal (1997) [36], Ben Rayana (2007) [37]. However, their calculated frequencies of the wavy instabilities were larger than the predicted values from inviscid stability analysis by a factor of 3 and from the growth rate by a factor of about 6. Matas et. al (2011) [35] improved the theoretical predictions by considering a velocity deficit at the liquid-gas interface

induced by the splitter plate and a finite gas thickness. It still, however, did not take into account the viscosity of the fluid. Otto et. al (2013) [38] incorporated viscous effects in the analysis and found three characteristic unstable modes. The results were compared against both the axisymmetric case of Marmottant and Villermaux (2004) [34] and the planar rectangular case of Matas et. al (2011) [35]. In the planar case, the flow was convectively unstable for all velocity defect widths when $\lambda < 0.9$. For greater λ, the flow became absolutely unstable for velocity defects smaller than 1. No favorable agreement was found when the velocity defect width equaled 1. In spite of the results being superior to the previous inviscid analysis, the experimental values were still higher than the predicted theoretical values at higher gas velocities.

Fuster et. al (2013) [14] then looked into two planar coflowing fluid sheets (air and water) by varying density and dynamic pressure ratios and identified three different flow regimes based on the flow behavior. Numerical simulations were carried out along with experiments conducted for water-air systems at high density ratios which were then compared with temporal and spatiotemporal linear stability analysis from Otto et. al (2013) [38]. Their work showed convergence between experiments, simulation, and linear stability analysis on surface tension induced absolute instabilities. In the experiments, the primary air velocity was fixed at 20 m/s and the secondary water velocity was altered to generate various dynamic pressure ratios, M in between 0.5 and 32. As the dynamic pressure ratio was increased, the flow went through a transition from convective to absolute instability and the observed frequencies became independent of the liquid velocity and liquid boundary layer. The effect of the velocity defect induced by the splitter plate was also explored in the study, and it was concluded that when splitter plate thickness was increased to become of the order of gas boundary layer thickness, most unstable frequencies got reduced with significant noise in the spectrum. At higher density ratios in the flow, the critical dynamic pressure ratio was found to be lower.

Matas et al. (2015) [39] showed that the gas turbulence in the form of velocity fluctuations directly influenced the shear instability of the planar air-water mixing layer. In two different experiments, it was established that increasing velocity fluctuations in the air increased the frequency of the instability, with the frequency almost doubling for the largest turbulence intensity. The observations matched with the spatiotemporal stability analysis when viscosity and confinement were taken into account.

3.3. Effect of Confinement

Yang et al. (2021) [40] looked into the confinement effects on the absolute and convective instabilities in countercurrent shear layers. Spatiotemporal linear stability theory was used to study effects of confinement on frequency, growth rate, wave number etc. at different velocity ratios and associated instability modes were investigated while incorporating the effects of wall boundary layer thickness. Later the analytically calculated frequencies were compared with experimentally observed peak frequencies. With the results, it was confirmed that momentum driven flows can in fact be used to create countercurrent shear layers in confined

flows without forming a stagnation point under appropriate operating conditions. Additional unstable long-wave modes appeared because of confining the walls. With increasing confinement, the original unconfined mode transitioned to convective instability and the long wave modes became dominant by becoming absolutely unstable while also decreasing in wavelength. Flow was confined both on the low speed and on the high-speed sides. It was found that high speed side confinement was much more destabilizing in comparison to the low-speed side. Even though the experimentally measured velocity profiles did not resemble the canonical tanh velocity profile, overall trends in the measured frequency are similar to that of the predicted values of the confined modes.

For water-air coflowing shear layers, confinement was proved to be a transition mechanism from convective to absolute instability by Bozonnet et al. (2022) [20]. Out of the three competing mechanisms discovered for destabilization by Matas et al. (2018) [41]: a convective instability, an absolute instability driven by surface tension and an absolute instability driven by confinement; the effect of confinement was studied by implementing finite liquid and gas stream thickness (H_l and H_g respectively) in the numerical calculations and showed convergence between experimental [35], analytical (Linear Stability Theory) and the computed numerical results, similar to the work of Fuster et. al (2013) [14] for surface tension induced instabilities. While the effect of both the fluid stream thicknesses (H_l, H_g) on frequency is symmetric, their effect on amplitude is not. At lower stream thickness, the mode remained convective whereas increasing the thickness, the mode became absolute. With symmetric confinement on either side ($H_l = H_g = H$) increasing the dynamic pressure ratio might trigger the absolute instability earlier at lower stream thickness. Wave frequency, f in confinement induced absolute modes was found to scale with ~ 1/H scaling which validates the scaling law obtained from Matas et al. (2018) [41]. For asymmetric confinement (H_l not equal to H_g) the frequency scales with the most restrictive confining length, $f \sim 1/\min(H_l, H_g)$.

4. Experimental Set-up

4.1. Facility Design

For this study, an experimental facility is designed and built with similar features to the momentum driven single-phase air facility used by Anderson (2011) [13]. However, there are still some fundamental differences and adjustments made during the design process. The schematic diagram of the facility is provided below:

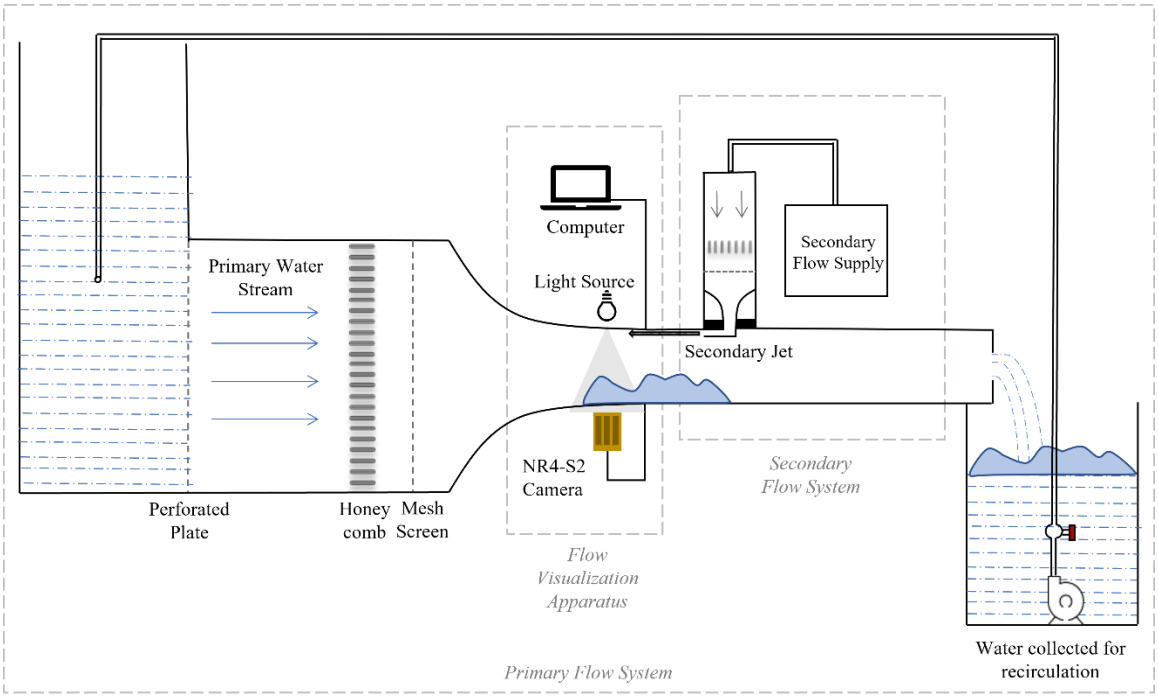

Figure 11-Schematic diagram of the experimental setup

The facility consists of primary and secondary flow delivery systems and flow visualization equipment. The facility runs in steady state constant flow rates. The primary channel is supplied with water first which is then recirculated and run at constant flow rates via a pump. Thus, a uniform flow in the study chamber is ensured. The flow can be regulated by a valve which is attached to the pump. The secondary jet supplies a fluid stream on top of the primary flow channel to establish a countercurrent shear layer in the study region. The jet can be either water or air depending on the nature of study that is to be conducted. The jet can also be moved along the length of the study channel which provides options to look at the spatial development of the shear layer. The interaction between the two streams can be studied via high-speed back illuminated imaging or Particle Image Velocimetry (PIV) which is controlled by a computer.

4.1.1. Primary Flow

The primary flow channel (Figure 11) was designed to be similar to the geometry - I from Anderson (2011) [13] in order to expand the current understanding of counterflow study for confined multiphase flows. From Figure 12 the design for the water channel has three major segments: (i) water tank, (ii) flow-conditioning region, and (iii) study channel. The whole system is used as a recirculation facility using a pump, once the tank is filled up initially with tap water (Figure 12). A 1.2 HP submersible pool pump capable of delivering 60 GPM is used for this purpose. A PVC ball valve is used to control the desired water supply into the study channel. With a maximum flow rate of 60 gallons per minute from the pump, the velocity in the channel comes to about 24.5 cm/s at the inlet of the channel giving a Reynolds number of about 17000. Following table shows the range of flowrates, their corresponding velocities and Reynolds numbers in the channel:

Table 1-Primary channel flow rates

Flowrate (gpm)	**Velocity (cm/s)**	**Reynolds Number**
0	0	0
3	1.22	852
6	2.44	1703
9	3.67	2555
12	4.89	3406
15	6.11	4258

For the tests conducted here, the primary flow rate was selected to be kept constant at 6 gpm for all the cases since the goal was to operate the primary flow rate near a Reynolds number of 1000. This translates into a velocity of about 2.5 cm/s in the channel providing a Reynolds number close to 1700. (Table 1)

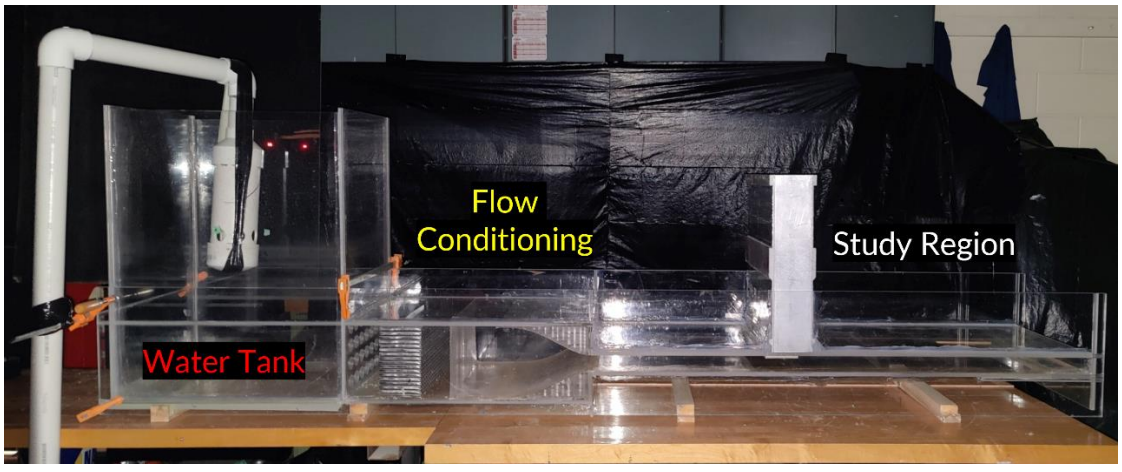

Figure 12 - Primary Flow Channel

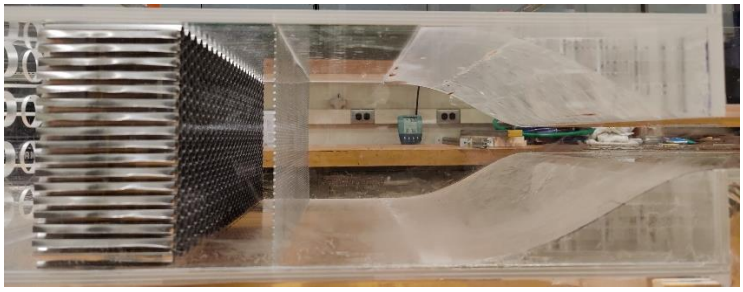

(a)

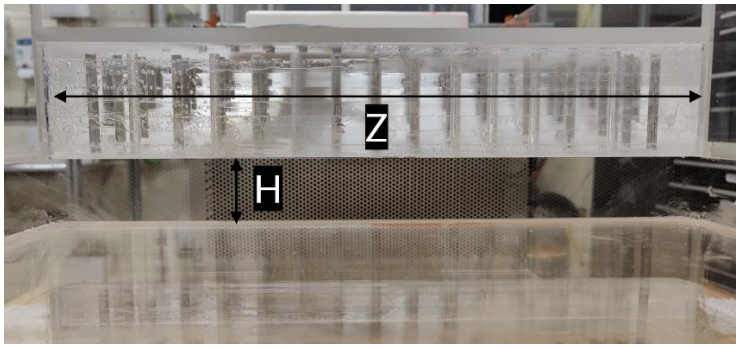

(b)

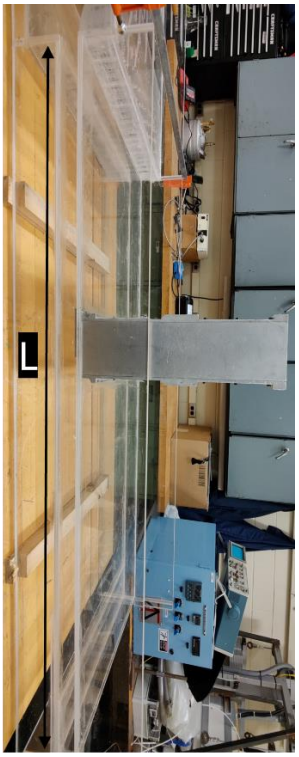

(c)

Figure 13 - (a) The flow conditioning region, (b) The width and depth of the study region, (c) The length of the study region

In the design, the vertical gravity fed water tank holds the water for recirculation and has a capacity of about 35 gallons. The goal is to get rid of any upstream disturbances in the flow channel. Therefore, the flow-conditioning region includes a perforated plate with 30 mm diameter holes, a honeycomb panel with 10 mm hexagonal cells, a mesh screen with 3 mm holes (Figure 13a). The variable outlet sizes dissipate the upstream turbulent eddies and provides smooth flow into the study channel. The screen is followed by a 14:3 two-dimensional nozzle, which was designed by fitting a quadratic polynomial shown below (Figure 14). The flow was assumed to be unidirectional along the nozzle having no velocity gradient in the y-direction providing uniform flow at the nozzle exit. This profile was used as the area contraction nozzle profile for both the primary and secondary flow delivery systems.

$$y = a + \frac{b - a}{L^4}[6x^2L^2 - 8x^3L + 3x^4]$$

where, a = Height of the nozzle at the inlet

b = Height of the nozzle at the outlet

L = Length of the nozzle

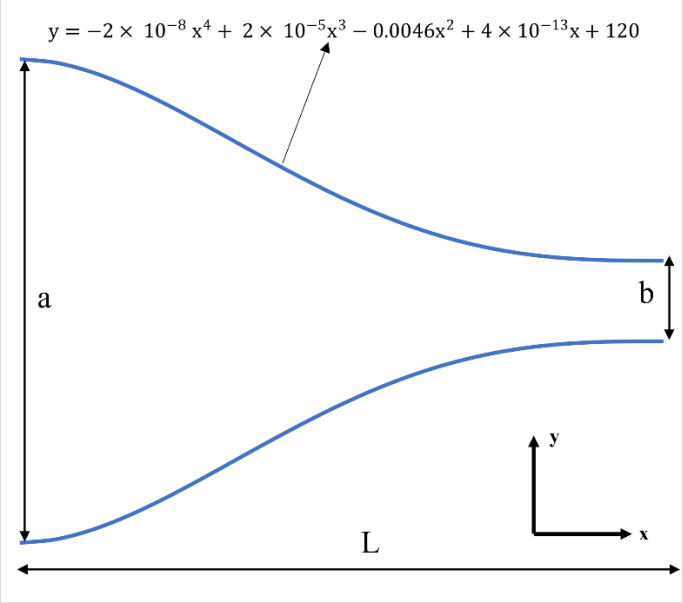

Figure 14 - Contraction profile

Incorporating the facility dimensions, the following equation is obtained:

$$y = -2 \times 10^{-8} x^4 + 2 \times 10^{-5} x^3 - 0.0046x^2 + 4 \times 10^{-13} x + 120$$

Figure 15 shows a schematic diagram of the study region of the facility. The height of the primary channel, H was kept constant throughout the test section as 1.5 inch (3.81 cm) since there were no splitter plates used to differentiate the two streams. This facility aims at studying the interaction between the primary and secondary streams in a more confined manner which is why the design does not include any splitter plates. The spanwise dimension was taken as, Z ~ 10.5H (16.25 inch or 41.275 cm). The width was carefully taken to be large enough to avoid any edge effects in the development of the shear layer. The length of the primary flow channel, L is 48 inch (121.92 cm). The end of the channel was partially blocked to ensure that the facility had enough water and flow rate in the system. Twelve holes of 5/32 inch (3.97 mm) diameter (l) were made on the backplate which provided enough backpressure in the system and kept the water level constant in the water tank during the tests. For the material, clear polycarbonate sheets of ½-inch and 3/8-inch thickness were machined and used inside the facility for better visibility during imaging and optical access.

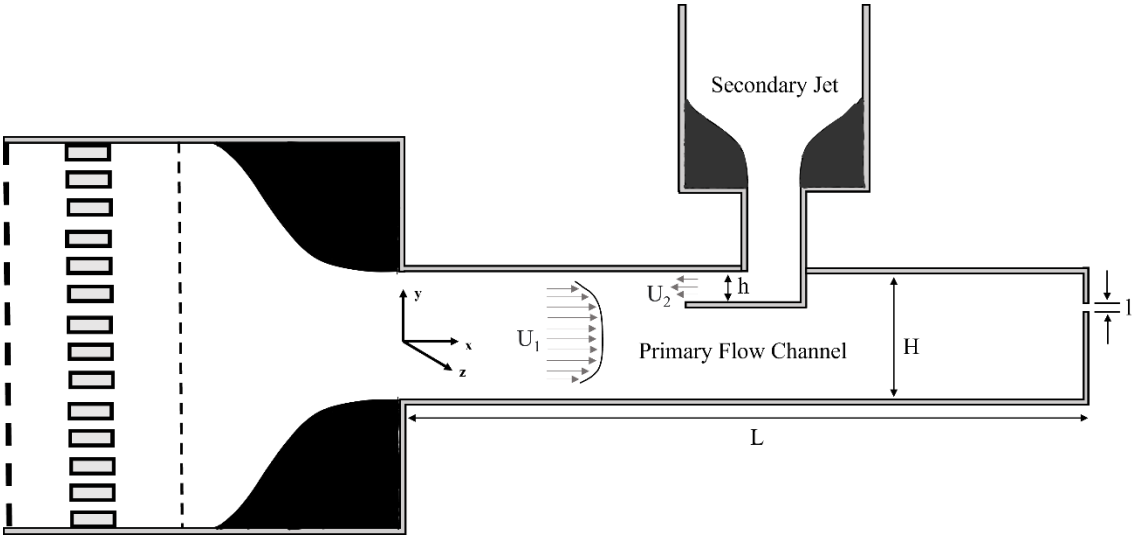

Figure 15- Study region of the facility

4.1.2. Secondary Flow

The secondary jet system consists of a plenum that houses the secondary stream flow conditioning and a flow delivery system. A diffuser delivers the flow from the pump into a 15 inch x 3.5 inch (381 mm x 89 mm) rectangular channel into a plenum that used two perforated plates for flow conditioning. The flow conditioning is similar to that of the primary channel and consists of a honeycomb panel (6 mm) and a screen (1.5 mm). (Figure 16) The height of the secondary jet, h in this system can be varied between 4 and 8 mm. The upstream and downstream distance of the secondary jet, d_1 and d_2 can be varied by changing different plates (Figure 17a). This positions the secondary jet at four different locations equally spaced in the channel along the streamwise direction. Another benefit of this design includes the possibility of using the facility both as a closed channel and a partially open channel setup (Figure 17). The plenum side plates were made from aluminum and the jet base plate was made from stainless steel.

(a)

(b)

(c)

(d)

Figure 16 - Secondary Flow Jet

In this design, the secondary jet seats on top of the primary flow channel thus facilitating studies both in a fully closed and partially open channel (Figure 17). This can be achieved by swapping out the adjacent polycarbonate plates to the jet delivery. The secondary jet is also capable of multiphase studies meaning it can either run water or air through it. For this purpose, the fluid delivery system needs to be changed.

Water is supplied to the secondary channel using a 20 GPM ⅙ HP submersible pump. This provides a maximum velocity of 80 cm/s out of the base plate. (Figure 18a) For secondary air flow, the facility will use an AB-600 Atlantic blower paired with a GS-2 AC drive for control, capable of delivering over 200 cfm. A Hedland variable area flow meter capable of measuring air flow from 0 to 250 cfm is attached along with an inlet pressure gauge. (Figure 18b) The experiments shown here used secondary water jet at 3, 6, and 12 gpm flow rates while the primary flow rate was kept constant. Following table shows the corresponding velocities and Reynolds numbers:

Table 2 - Secondary jet flow rates

Flowrate (gpm)	**Velocity (cm/s)**	**Reynolds Number**
0	0	0
3	12.42	983
6	24.84	1966
9	37.26	2950
12	49.68	3933
15	62.10	4916

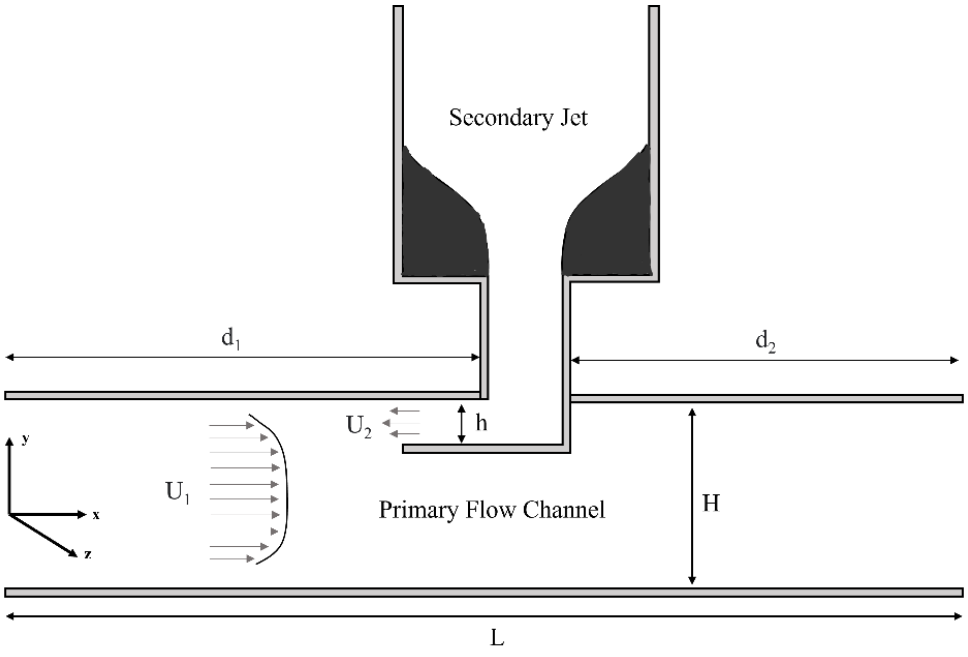

(a)

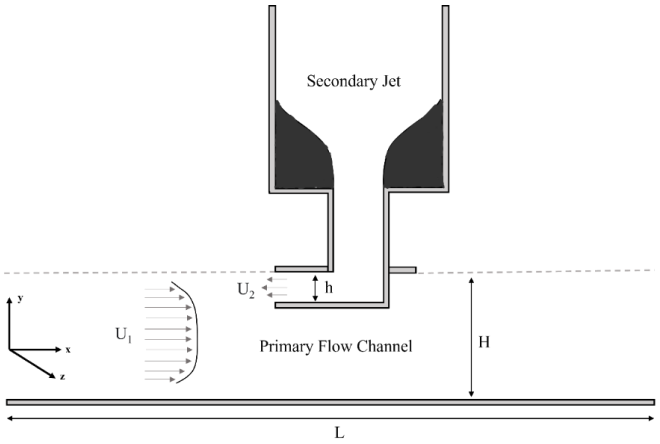

(b)

Figure 17 – (a) Closed channel facility, (b) Partially open channel facility

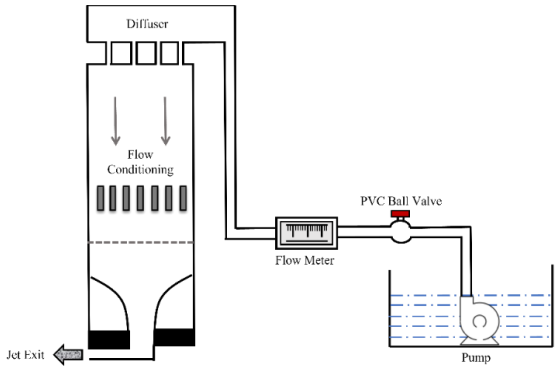

(a)

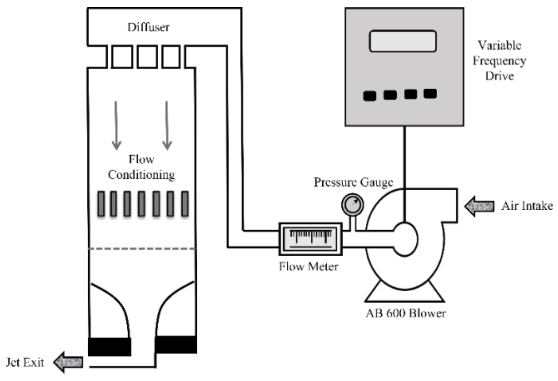

(b)

Figure 18 – (a) Water jet delivery system (b) Air jet delivery system

4.2. Imaging and Flow Visualization

For flow visualization, the system is equipped with an IDT NR4S2 camera capable of recording at 2000 fps at 1024 x 1024 resolution. The camera is paired with a Nikon Sigma 105 mm f2.8 macro telephoto lens. A Teleplus Pro 300 1.4x DGX teleconverter is used to obtain clear images of the flow domain with a magnification factor of 1.4. This combination provided a clear macroscopic field of view of the secondary jet exit. To properly visualize the flow behavior, liquid dye (food color) was used in most cases. In all the cases, the imaging field was illuminated via a light source which was placed directly behind the flow channel in line with the camera. Frame rates were varied between 90-200 frames per second to obtain 900-1000 images in a single run with fixed primary and secondary flow rates. The focal length, aperture, and exposure settings were adjusted accordingly in each case.

The overall flow field and interactions between the two streams were recorded via a mobile phone camera which included a three-camera array. A 48 megapixel 1/1.43 inch Sony IMX789 f/1.8 sensor was used as the main camera along with a 50 megapixel 1/1.56 inch Sony IMX766 f/2.2 ultra-wide camera. The telephoto camera was 8 megapixel and with a f/2.4 aperture. White background was used and the secondary jet was injected with blue dye during the imaging process. The phone was mounted on top and side to provide a sharp clear view of the flow interactions. All the videos were recorded at 4K 120 fps to retain the clarity and slow-motion capabilities.

5. Results

In this section, the results of the initial experiments are reported. Flow visualization was implemented to obtain quantitative and qualitative results from the facility. The facility operated with a primary and a secondary flow which interacted at different flow rates. For the initial tests, both the primary and secondary flows were run with water. To ensure steady state conditions, the primary flow was run at least ten minutes. After ensuring steady state conditions for primary flow, secondary stream was turned on and recorded via a camera. Blue dye was injected in the secondary stream for flow visualization. For all cases, the primary flow rate was fixed at 6 gpm. Three different secondary flow rates were tested at 6 gpm (Case – I), 3 gpm (Case – II), and 12 gpm (Case – III) which provided different shear layer growths.

Table 3 - Three different cases with different flow rates

	Primary Flow Rate (GPM)	**Secondary Flow Rate (GPM)**
Case I	6	6
Case II	6	3
Case III	6	12

5.1. Case - I

For the first test case (Case – I), both the primary and secondary flow had a flow rate of 6 gpm which provided a velocity ratio, r = 10. ($r = U_2 / U_1$) As the flow comes out of the secondary jet, initially it turns completely after travelling 3.5 inches at t = 1.0 s (from the scale attached in the image) (Figure 19a). The primary stream pushes on the secondary stream thus fluctuating the interface between them. The momentum of the two streams is diffused at the interface giving rise to vortices and fluctuations. The secondary flow then advances upstream interacting with the primary stream (Figure 19b,c,d). Near the top wall, the momentum of the jet is higher. This is why the flow travels farther upstream near the top wall in comparison to the bottom wall. As the jet reaches the maximum distance upstream (the penetration length), the flow starts to turn back and interfacial wave patterns can be seen (Figure 19e). The penetration length in this case is 14.5 inches. The wave patterns at the interface are ultimately convected downstream reducing the shear layer thickness also creating vortices due to the primary stream interaction (Figure 19f,g,h). Once steady-state is achieved, the shear layer thins at the point of maximum penetration. (Figure 19i)

Figure 20 reveals a close-up image of the secondary jet exit and the secondary flow turning while establishing a countercurrent shear layer. Initially, the jet starts to turn as soon as it leaves the jet exit (Figure 20a). It takes the jet around 1.0 second to turn completely. With time, as the jet interacts more with the primary flow and momentum is transported from the primary flow, it attaches itself to the top wall and therefore further advances upstream taking a longer distance to turn. Figure 20b and c show the gap between the top plate and the secondary jet is getting reduced as the flow is attaching itself to the top wall. The interface between the primary and secondary flow exhibits flapping motion near the exit as the secondary flow leaves the jet. Figure 20d shows a fully attached secondary jet which has travelled farther distance upstream.

(a)

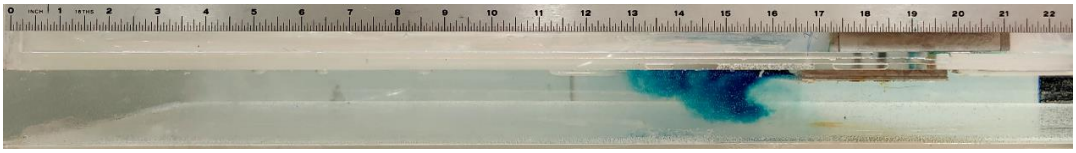

(b)

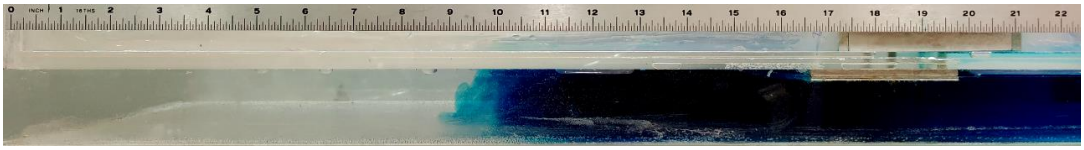

(c)

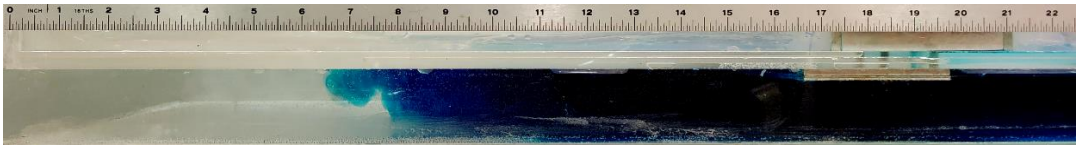

(d)

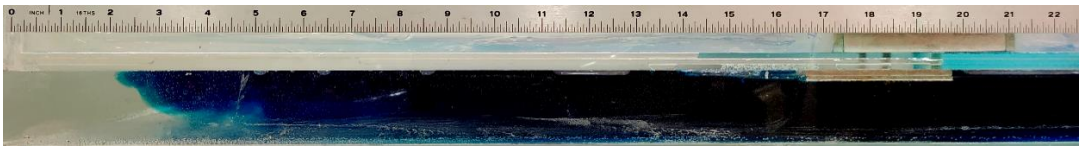

(e)

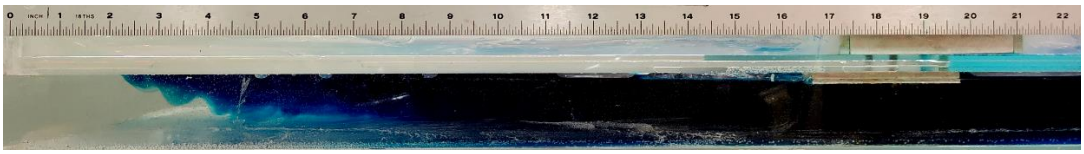

(f)

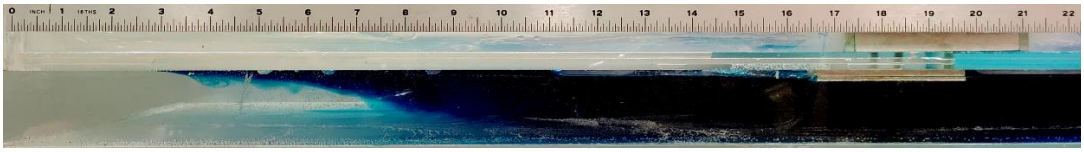

(g)

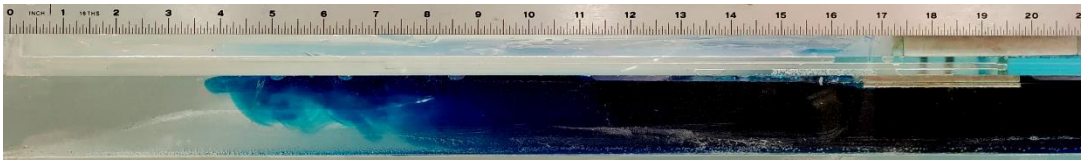

(h)

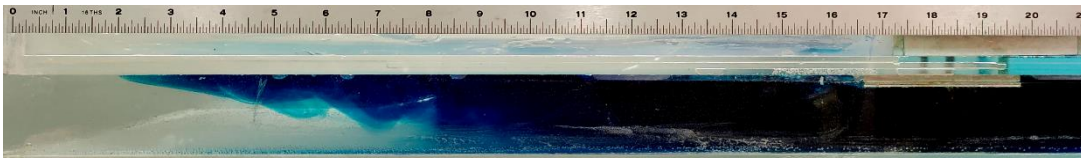

(i)

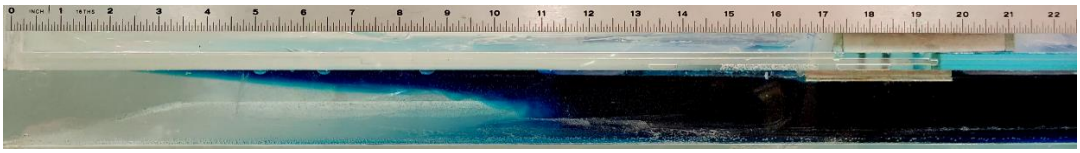

Figure 19 - Development of countercurrent shear layer from side at 6 gpm primary and 6 gpm secondary flow rate at (a) t = 1.0s, (b) t = 11.0s, (c) t = 16.0s, (d) t = 35.0s, (e) t = 45.0s, (f) t = 55.0s, (g) t = 78.0s, (h) t = 100.0s (i) t = 115.0s

(a) (b)

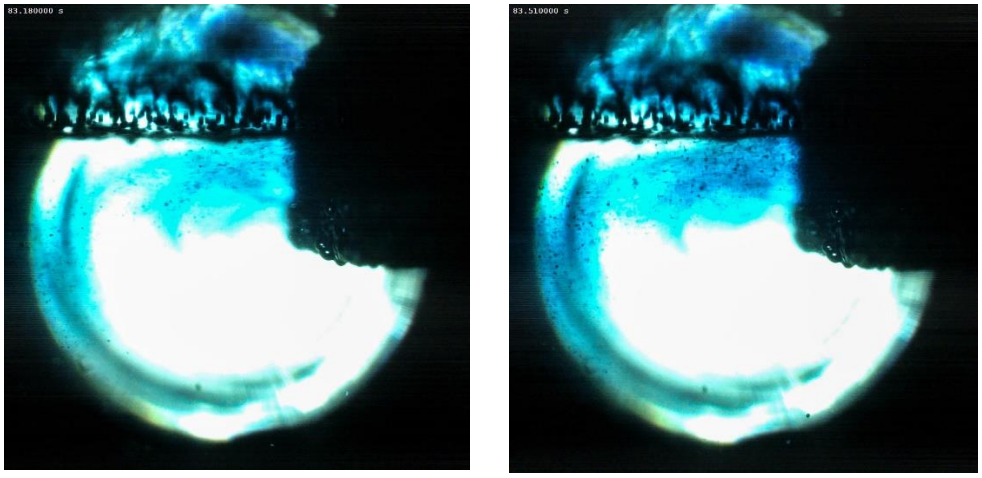

(c) (d)

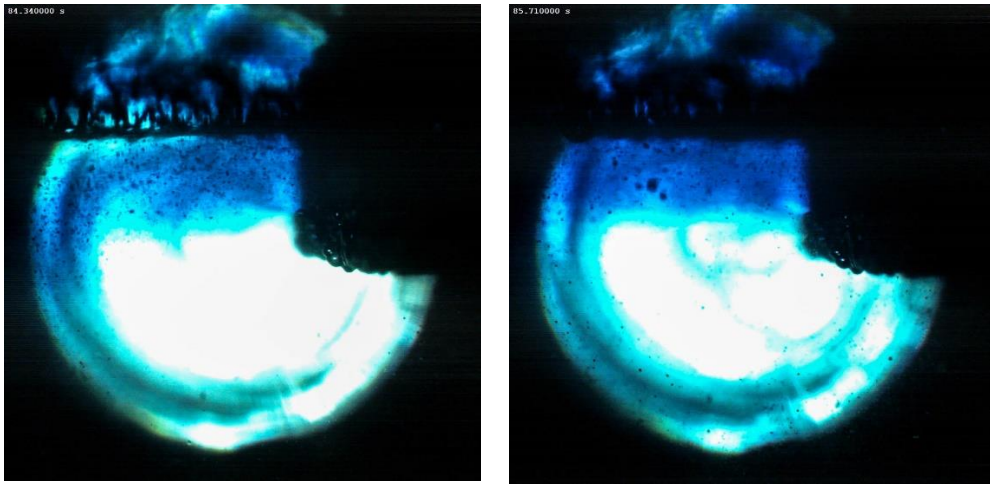

Figure 20 - Secondary flow near the jet exit at (a) t = 0.68s, (b) t = 1.01s, (c) t = 1.84s, (d) t = 3.21s

Images of the span view shows that the secondary flow is uniform near the jet exit (Figure 21a). As the secondary jet advances upstream, it does not stay uniform (Figure 21d,e). The two flows give rise to unique flow structures after interaction. These images also show that the flow structures are somewhat uniform in the beginning (Figure 21b,c) and with time the flow structures roll and twist along the span indicating strong three dimensionality. Upon a closer look at the Figure 21f and g, a recirculation zone develops in the center of the span. As a combination of these effects, the secondary flow progresses in two peaks on the two corners with a gap in the middle (Figure 21f). The size of the recirculation zone is unclear from the images. It causes the two peaks to spiral outwards near the center of the jet. With time, the dye was mixed throughout the span upstream not making it possible to deduce further flow features beyond t = 38.0 s.

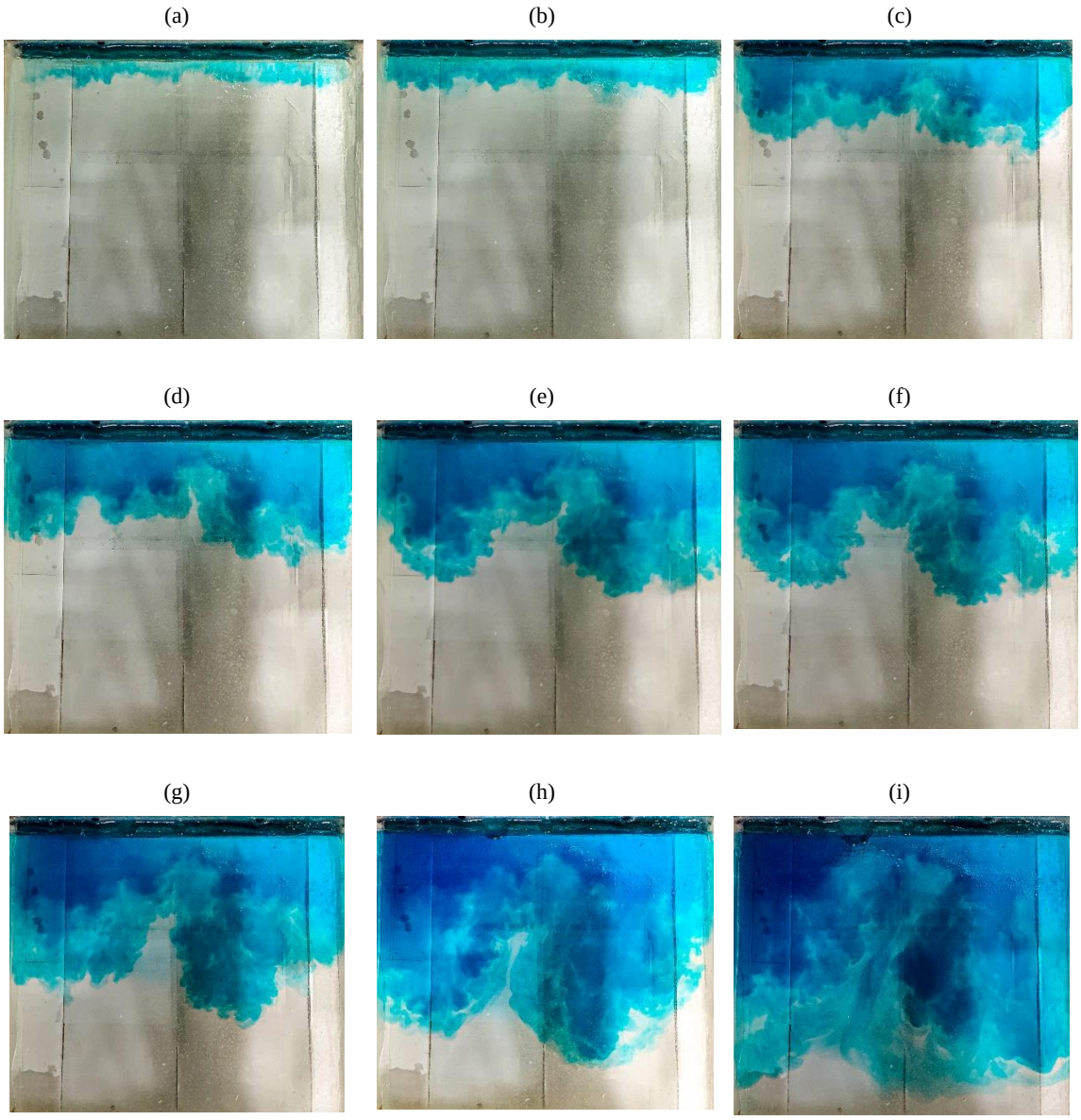

Figure 21 – Span development of countercurrent shear layer at 6 gpm primary and 6 gpm secondary flow rate at (a) t = 1.0s, (b) t = 3.0s, (c) t = 8.0s, (d) t = 10.0s, (e) t = 13.0s, (f) t = 15.0s, (g) t = 20.0s, (h) t = 30.0s, (i) t = 38.0s

5.2. Case - II

For case-II, the secondary flow rate was reduced to 3 gpm giving a velocity ratio (r) of 5. As a result, the flow turns faster initially near the jet exit, only after travelling 1.5 inches at t = 0.5s. (Figure 22a). The secondary flow does not have as much momentum as the previous case. This results in longer time for the secondary flow to travel upstream. Also, the flow near the top wall is not as fast since the jet velocity is lower. Thus, advancing faster near the bottom wall in a lot of instances. (Figure 22b) Whenever, the jet near the top wall is able to catch up, vortices are formed because of the flow confinement in the top wall. (Figure 22c,d,f) At the interface between the two streams, wave patterns are found but for shorter duration in comparison to the previous case. The wavelength at the interface is shorter in this case than the higher secondary flow rate case. (Figure 22e,g,h). With time the flow near the top wall is continuously trying to catch up with the flow near the bottom wall. Thus, not resulting in a stable interface like Case - I (Figure 22i). The maximum length the secondary flow advances upstream, or, the penetration length in this case is 7.5 inches. (Figure 22e)

(a)

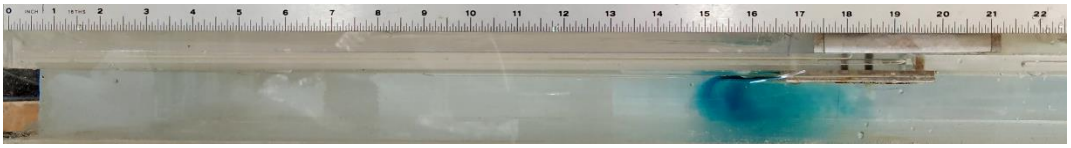

(b)

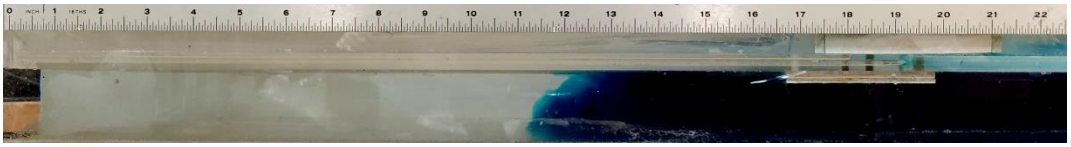

(c)

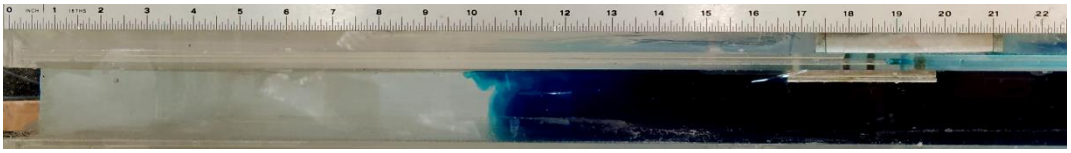

(d)

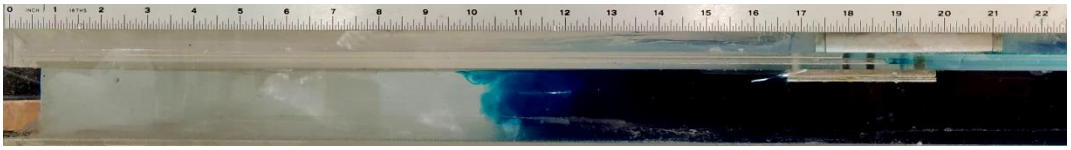

(e)

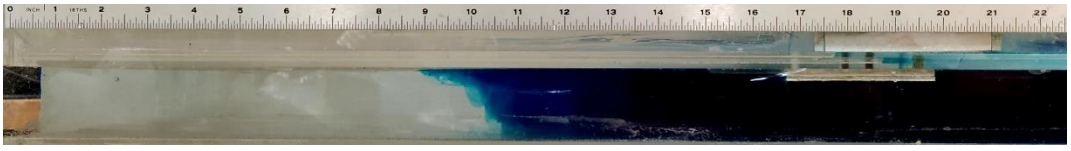

(f)

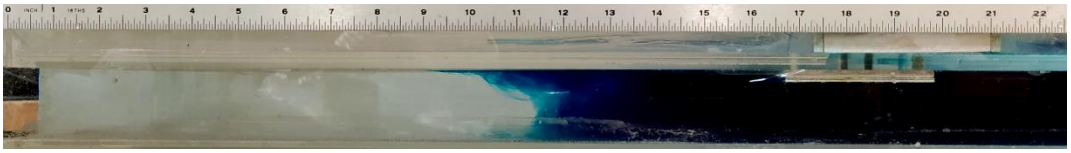

(g)

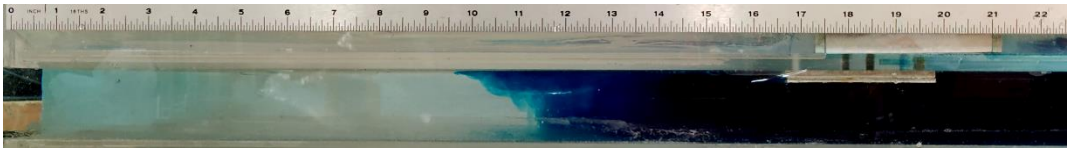

(h)

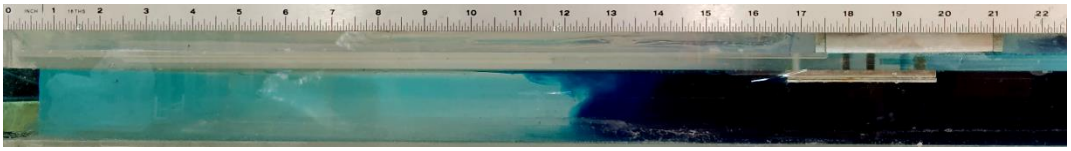

(i)

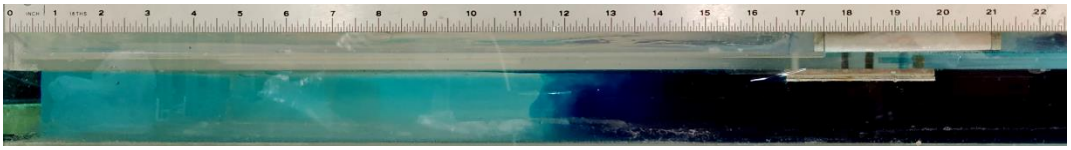

Figure 22 - Development of counterflow shear layer from side for 6 gpm primary and 3 gpm secondary flow rate at (a) t = 0.5s, (b) t = 26.0s, (c) t = 66.0s, (d) t = 70.0s, (e) t = 90.0s, (f) t = 100.0s, (g) t = 130.0s, (h) t = 140.0s, (i) t = 194.0s

Similar to the span view in case-I, the secondary flow starts uniformly near the jet exit (Figure 23a). Soon after the flow interacting with the primary stream, flow structures appear. The flow structures are non-uniform along the span. In the beginning the structures appear like two peaks near the two edges. The rolling and twisting motion of the flow structures causes one of the peaks to advance more on the right-hand side indicating the flow might not be uniform along the span because of three-dimensionality. As a result, the secondary flow becomes dominant near the right-hand side penetrating more in comparison to the other side. Ultimately, the flow turns and moves enough to shift the dominant peak to the center. This indicates the flow to be more three-dimensional on one side and thus dissipating not uniformly across the length and depth of the facility. The secondary flow in this case is not as uniform as the previous case suggesting the flow is more three-dimensional when secondary flow rate was lowered.

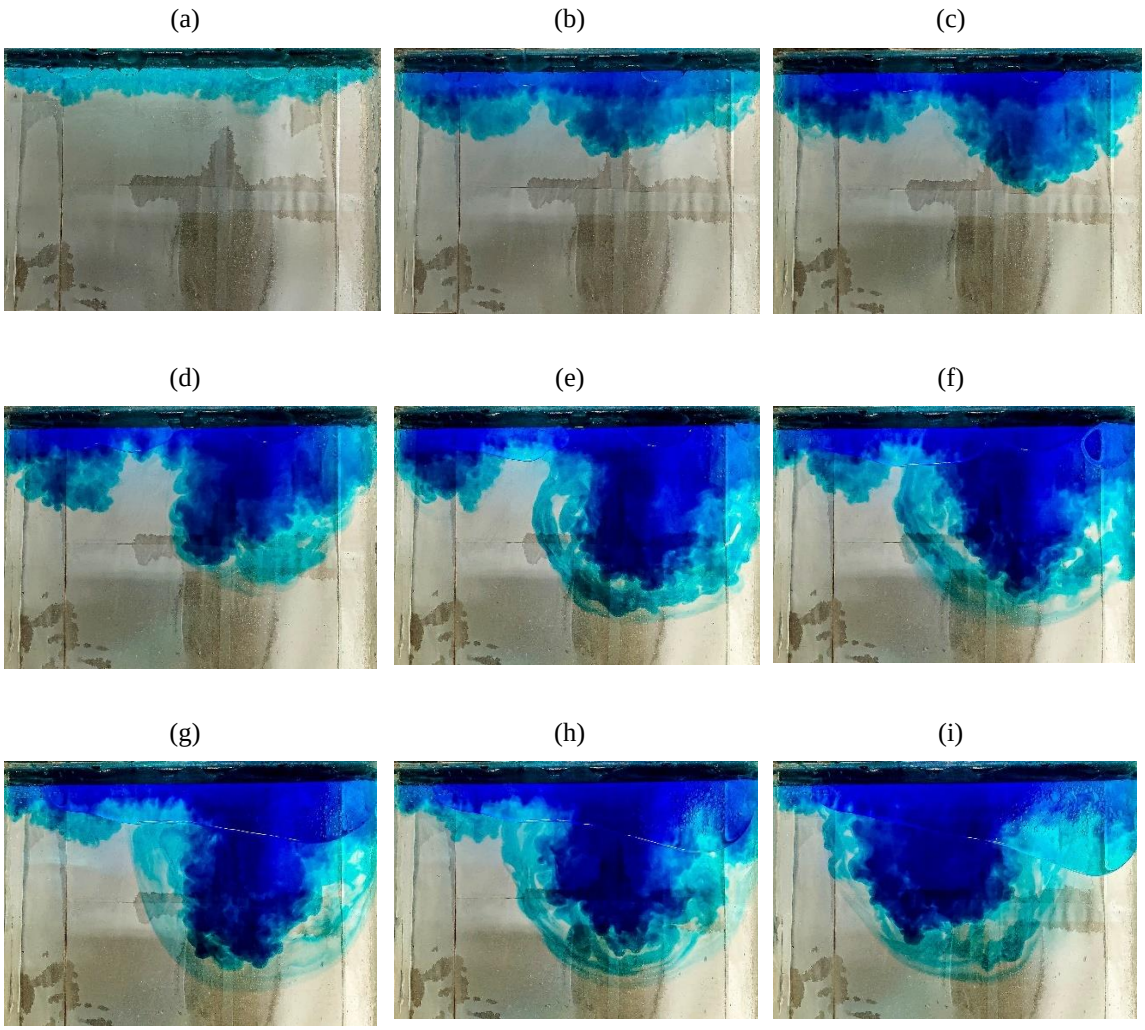

Figure 23 - Development of counterflow shear layer from top for 6 gpm primary and 3 gpm secondary flow rate at (a) t = 2.0s, (b) t = 18.0s, (c) t = 30.0s, (d) t = 40.0s, (e) t = 50.0s, (f) t = 55.0s, (g) t = 65.0s, (h) t = 80.0s, (i) t = 90.0s

5.3. Case – III

For the last case, the secondary flow rate was increased from 6 gpm in Case I and 3 gpm in Case II to 12 gpm giving a velocity ratio of 20. The higher flow rate caused bubbles to get trapped on the top plate near the jet exit (Figure 24a). The test was repeated multiple times to avoid this. However, similar results were observed every time. This could mean the bubbles were generated inside the secondary jet because of the higher flow rate inside the flow delivery system or it could be created as a result of the flow interaction at higher velocity. Since the momentum of the jet is higher in this case, the flow took a while to turn initially. (Figure 24b,c) The secondary flow travelled 5.5 inches upstream before turning completely from the jet exit. The secondary flow in this case is significantly faster than the other two cases. It takes the secondary flow only about 15 seconds to reach the origin (Figure 24e). The high-speed secondary jet travel significantly faster and therefore

facilitates rapid mixing at the interface between the two streams. Unlike the previous cases where the secondary flow travelled upstream while being attached to the top wall and stopping ultimately at the penetration length, this time the high velocity of secondary jet allowed it to enter the inlet nozzle and flow conditioning region (Figure 24f,g). Therefore, the whole channel was soon filled with blue dye (Figure 24h). No flow structures and wave patterns could be seen like the previous two cases.

(a)

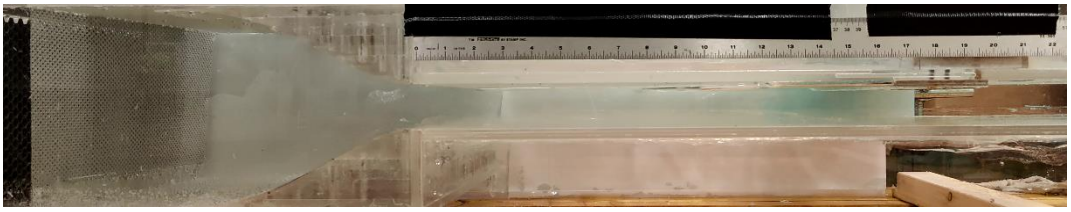

(b)

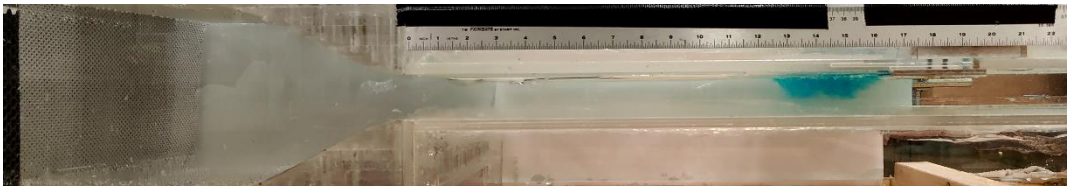

(c)

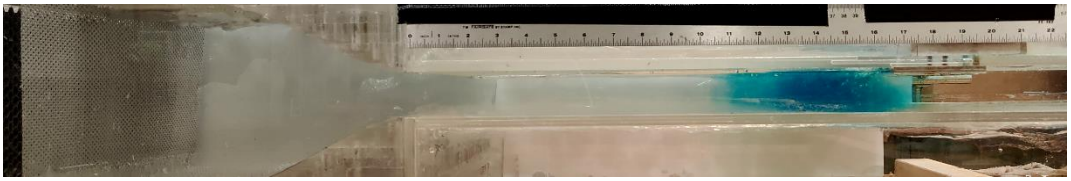

(d)

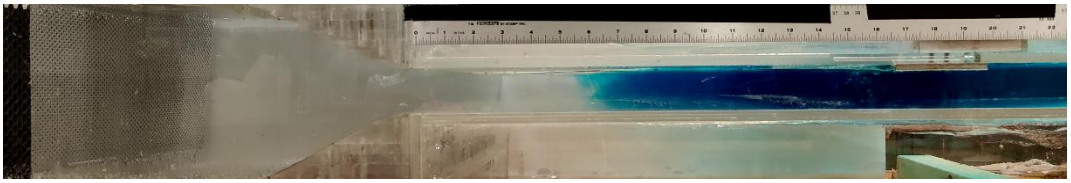

(e)

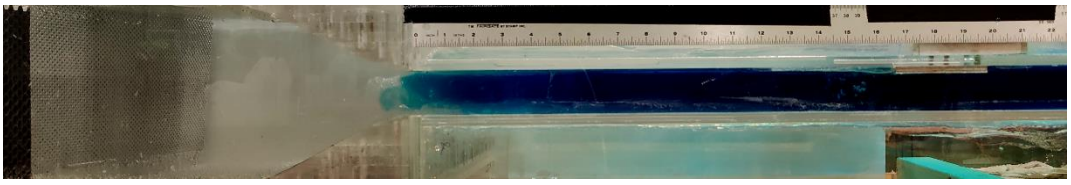

(f)

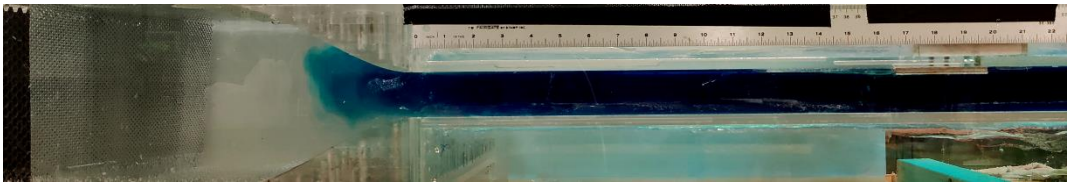

(g)

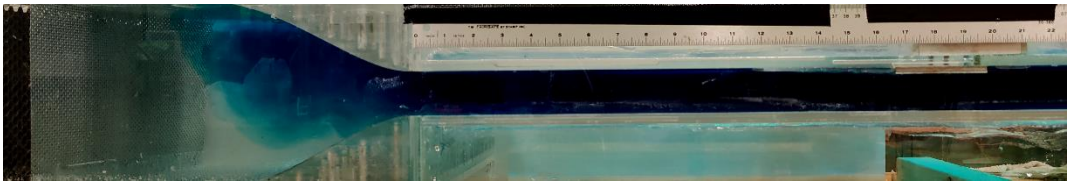

(h)

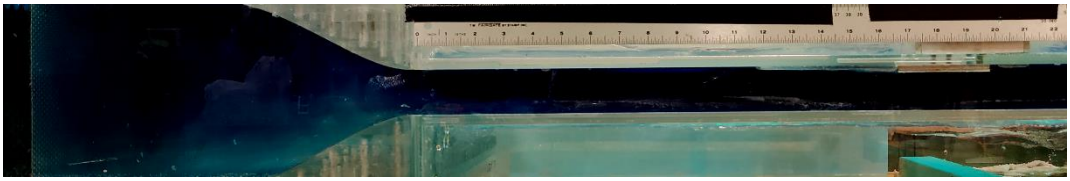

Figure 24 - Development of counterflow shear layer from side for 6 gpm primary and 12 gpm secondary flow rate at (a) t = 1.0s, (b) t = 2.0s, (c) t = 2.75s, (d) t = 8.75s, (e) t = 17.0s, (f) t = 22.25s, (g) t = 29.25s, (h) t = 45.0s

The span view of case III shows the secondary flow advancing upstream from the jet exit. The flow is uniform at the jet exit in the beginning similar to the other two cases (Figure 25a). The entrained air bubbles can be seen in all the images. The higher flow rate of the secondary jet creates flow structures that are rapid and somewhat uniform. It still lacks the uniformity around the right edge (Figure 25d,e,f). The flow advances along the center and rolls towards the sides. In the end, the whole region is filled with dye because of the mixing (Figure 25i). The flow in this case is the most uniform along the span.

(a) (b) (c)

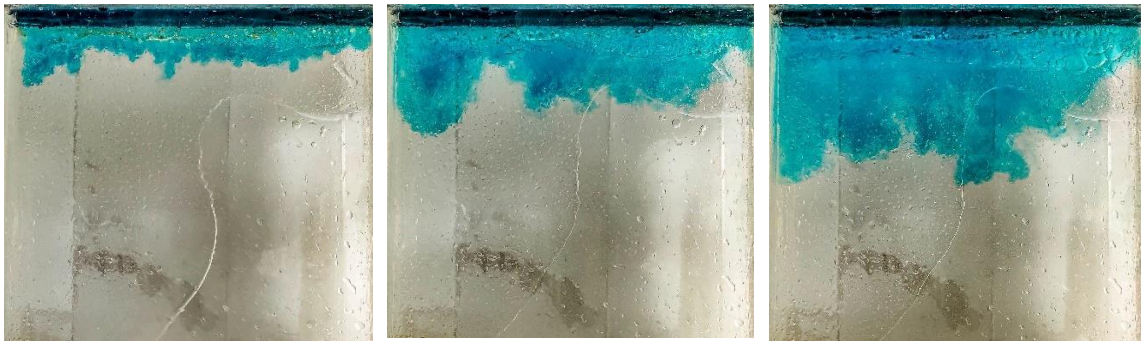

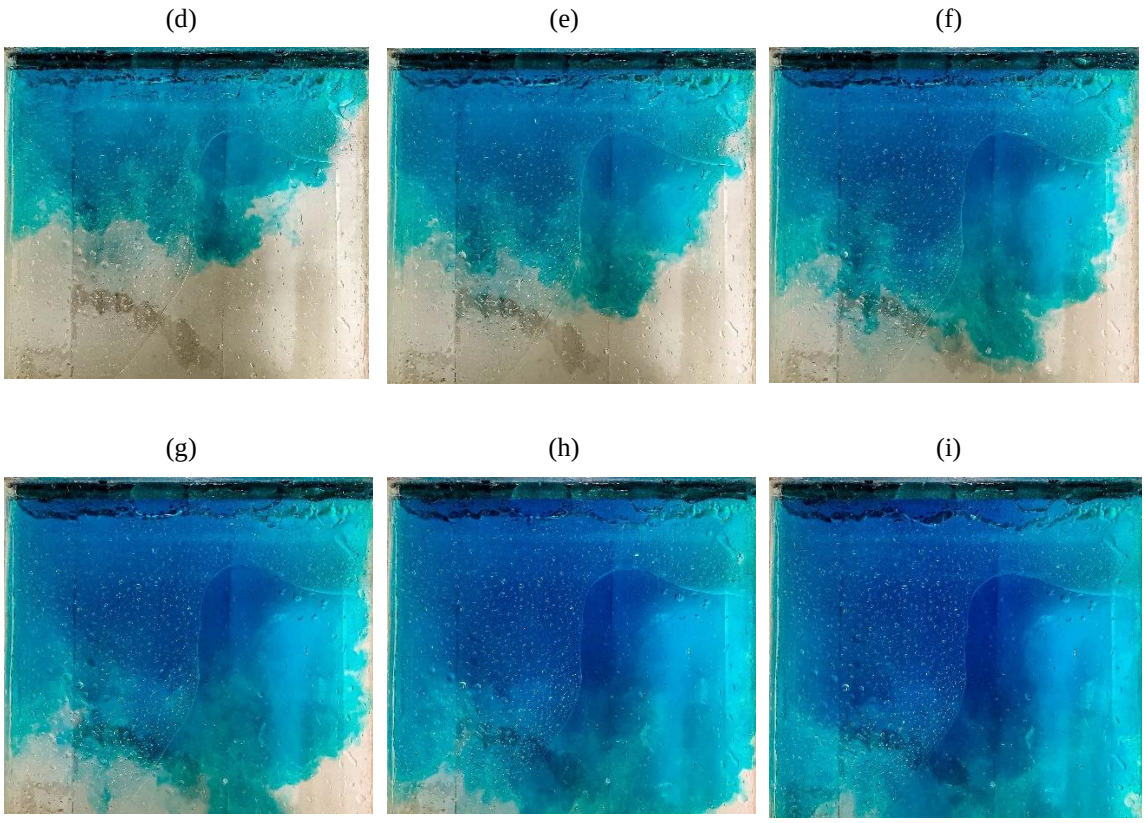

Figure 25 - Development of counterflow shear layer from top for 6 gpm primary and 12 gpm secondary flow rate at (a) t = 1.75s, (b) t = 2.5s, (c) t = 4.0s, (d) t = 7.5s, (e) t = 8.5s, (f) t = 12.0s, (g) t = 14.0s, (h) t = 16.5s, (i) t = 18.0s

To summarize, out of the three cases, case – III had the highest penetration length where the flow travelled all the way to the inlet nozzle (more than 16.5 inches). Case I and II had penetration lengths of 14.5 and 7.5 inches. This reflects the fact that case III had the highest secondary jet velocity and then case I and II subsequently. The order was also same where case III, I, and II had the travelling distance of 5.5, 3.5, and 1.5 inches subsequently before the flow turned from the jet exit initially. Case I and II had wave patterns developing after the flow travelled maximum distance upstream where the higher flowrate had longer wavelength at the interface.

In all three cases, the flow was not fully uniform along the span. Flow structures were developed because of the twisting and rolling of the flows. This caused flow three dimensionality in all three flow rates that were studied. However, case II had the maximum number of fluctuating structures and case III had the least. So, higher flow rates caused less three dimensionality in the experimental facility.

6. Conclusion & Future Work

An experimental facility was designed and built with similar features like Anderson (2011) [13] to establish countercurrent shear layer between primary and secondary fluid streams. The setup can be used for multiphase studies only by swapping out the fluid delivery method. The secondary jet location can be varied along the length of the study channel thus facilitating experiments at different locations. The top plate of the facility can be removed which optimizes the use of the facility both as closed (fully confined) channel and partially open channel.

Three different secondary flow rates were tested while keeping the primary flow constant. Flows were imaged using a high speed back illuminated camera along with a mobile phone camera array. Increasing the secondary flow rate increased the velocity of secondary jet which resulted in the flow turning late initially closer to the top plate and jet exit. On the other hand, the penetration length increased as a result of the secondary flow rate increasing. In spite of designing carefully, the experiments were not free of three-dimensional flow. Flow structures appeared in the span view in all the cases. However, the three-dimensionality was lesser at the higher flow rates.

In future, further studies are proposed by varying the jet location along the channel. The effect of confinement can also be found out by running the experiments in an almost fully open channel configuration with the shorter top plates. Lastly, the goal will be trying out multiphase studies where the secondary jet will be air. This will help in discovering the effect of density ratio in similar studies.

Lastly, forcing studies and stability analysis will reveal the stability of the shear layer which could provide further important insights into the flow domain and the interactions between the two streams. This could ultimately shed light into the breakup mechanisms inside the counterflow nozzle that was discussed in the introduction.

Reference

[1] A. H. Lefebvre and V. G. Mcdonell, *Atomization and Sprays*. CRC Press, 2017.

[2] A. Hoxie, E. Johnson, V. Srinivasan, and P. Strykowski, "Characterization of a Novel Energy Efficient Atomizer Employing Countercurrent Shear," in *14th International Conference on Liquid Atomization and Spray Systems, ICLASS 2018.*, 2020, pp. 1–9.

[3] S. D. Sovani, P. E. Sojka, and A. H. Lefebvre, "Effervescent atomization," *Prog. Energy Combust. Sci.*, vol. 27, no. 4, pp. 483–521, 2001, doi: 10.1016/S0360-1285(00)00029-0.

[4] B. M. Simmons and A. K. Agrawal, "Spray Characteristics of a Flow-Blurring Atomizer," *At. Sprays*, vol. 20, no. 9, pp. 821–835, 2010.

[5] R. Rangarajan, H. Zhang, A. Hoxie, and S. Yang, "Atomization of High Viscosity Liquids Using a Two-Fluid Counterflow Nozzle : Experiments and Modeling," *Turbo Expo Power Land, Sea, Air*, vol. 84133, p. V04BT04A022, 2020, doi: 10.1115/GT2020-15691.

[6] B. S. A. Thorpe, "Experiments on the instability of stratified shear flows : miscible fluids," *J. Fluid Mech.*, vol. 46, no. part 2, pp. 299–319, 1971.

[7] S. A. Thorpe, "A method of producing a shear flow in a stratified fluid A method of producing a shear flow i n a stratified fluid," *J. Fluid Mech.*, vol. 32, no. 4, pp. 693–704, 1968, doi: 10.1017/S0022112068000972.

[8] J. A. C. Humphrey and S. Li, "Tilting, Stretching, Pairing and Collapse of Vortex Structures in Confined Counter-Current Flow," pp. 466–470, 1981.

[9] F. S. Alvi, A. Krothapalli, and D. Washington, "Experimental Study of a Compressible Countercurrent TYirbulent Shear Layer," *AIAA J.*, vol. 34, no. 4, pp. 728–735, 1996.

[10] D. J. Forliti, B. A. Tang, and P. J. Strykowski, "An experimental investigation of planar countercurrent turbulent shear layers," *J. Fluid Mech.*, vol. 530, pp. 241–264, 2005, doi: 10.1017/S0022112005003642.

[11] D. L. Niccum, "The influence of velocity ratio on a counterflowing circular jet," University of Minnesota, 1990.

[12] D. J. Forliti, "Controlling dump combustor flows using countercurrent shear," University of Minnesota, 2001.

[13] M. J. Anderson, "Global Dynamics of a Dump Combustor Using Momentum - Driven Countercurrent Shear Control," University of Minnesota, 2011.

[14] D. Fuster *et al.*, "Instability regimes in the primary breakup region of planar coflowing sheets," *J. Fluid Mech.*, vol. 736, pp. 150–176, 2013, doi: 10.1017/jfm.2013.536.

[15] J. Yang, M. J. Anderson, P. J. Strykowski, and V. Srinivasan, "Effects of confinement on absolute and convective instabilities for momentum-driven countercurrent shear layers," *Phys. Rev. Fluids*, vol. 6, no. 7, 2021, doi: 10.1103/PhysRevFluids.6.073901.

[16] B. W. Spencer, "Statistical investigation of turbulent velocity and pressure fields in a two-stream mixing layer," University of Illinois at Urbana-Champaign, 1970.

[17] A. K. M. F. Hussain and M. F. Zedan, "Effects of the initial condition on the axisymmetric free shear layer : Effects of the initial momentum thickness," vol. 1100, no. 1978, 2012, doi: 10.1063/1.862349.

[18] C. Ho and L. Huang, "Subharmonics and vortex merging in mixing layers," *J. Fluid Mech.*, vol. 119, pp. 443–473, 1982.

[19] P. Huerre and P. A. Monkewitz, "Local and Global Instabilities in Spatially Developing Flows," *Annu. Rev. Fluid Mech.*, vol. 22, no. 1, pp. 473–537, 1990.

[20] C. Bozonnet, J.-P. Matas, G. Balarac, and O. Desjardins, “Stability of an air – water mixing layer : focus on the confinement effect,” *J. Fluid Mech.*, vol. 933, no. A14, 2022, doi: 10.1017/jfm.2021.1069.

[21] G. L. Brown and A. Roshko, “On density effects and large structure in turbulent mixing layers,” *J. Fluid Mech.*, vol. 64, no. 4, pp. 775–816, 1974, doi: 10.1017/S002211207400190X.

[22] B. Dziomba and H. E. Fiedler, “Effect of initial conditions on two-dimensional free shear layers,” *J. Fluid Mech.*, vol. 152, pp. 419–442, 1985.

[23] R. D. Mehta and R. V. Westphal, “Near-field turbulence properties of single-and two-stream plane mixing layers,” *Exp. Fluids*, vol. 4, no. 5, pp. 257–266, 1986.

[24] P. Huerre and P. A. Monkewitz, “Absolute and convective instabilities in free shear layers,” *J. Fluid Mech.*, vol. 159, pp. 151–168, 1985.

[25] P. J. Strykowski and D. L. Niccum, “The stability of countercurrent mixing layers in circular jets,” *J. Fluid Mech.*, vol. 227, pp. 309–343, 1991.

[26] S. Pavithran and L. G. Redekopp, “The absolute-convective transition in subsonic mixing layers,” *Phys. Rev. Fluids A Fluid Dyn.*, vol. 1, no. 10, pp. 1736–1739, 1989, doi: 10.1063/1.857496.

[27] P. J. Strykowski and D. L. Niccum, “The influence of velocity and density ratio on the dynamics of spatially developing mixing layers,” *Phys. fluids. A, Fluid Dyn.*, vol. 4, no. 4, pp. 770–781, 1992.

[28] A. S. D. Khemakhem, “An experimental study of turbulent countercurrent shear layers,” University of Minnesota, 1997.

[29] D. A. Hammond and L. G. Redekopp, “Local and global instability properties of seperation bubbles,” *Eur. J. Mech.*, vol. 17, no. 2, pp. 145–164, 1998.

[30] P. Yecko, S. Zaleski, and J.-M. Fullana, “Viscous modes in two-phase mixing layers,” *Phys. Fluids*, vol. 14, no. 12, pp. 4115–4122, 2002.

[31] P. Yecko and S. Zaleski, “Transient growth in two-phase mixing layers,” *J. Fluid Mech. fluid Mech.*, vol. 528, pp. 43–52, 2005.

[32] T. Boeck and S. Zaleski, “Viscous versus inviscid instability of two-phase mixing layers with continuous velocity profile,” *Phys. fluids*, vol. 17, no. 3, 2005.

[33] J. Eggers and E. Villermaux, “Physics of liquid jets,” *Reports Prog. Phys.*, vol. 71, no. 3, p. 036601, 2008.

[34] P. H. Marmottant and E. Villermaux, “On spray formation,” *J. Fluid Mech.*, no. 498, pp. 73–111, 2004, doi: 10.1017/S0022112003006529.

[35] J. P. Matas, S. Marty, and A. Cartellier, “Experimental and analytical study of the shear instability of a gas-liquid mixing layer,” *Phys. Fluids*, vol. 23, no. 9, 2011, doi: 10.1063/1.3642640.

[36] L. Raynal, “Instability and entrainment at the interface of a layer of liquid-gas mixture.,” Joseph Fourier University, 1997.

[37] F. Ben Rayana, “Contribution to the study of liquid-gas interfacial instabilities in assisted spray and drop size,” Instituto Politécnico Nacional de Grenoble (Grenoble INP), 2007.

[38] T. Otto, M. Rossi, T. Boeck, T. Otto, M. Rossi, and T. Boeck, “Viscous instability of a sheared liquid-gas interface : Dependence on fluid properties and basic velocity profile Viscous instability of a sheared liquid-gas interface : Dependence on fluid properties and basic velocity profile,” *Phys. Fluids*, vol. 25, no. 3, 2013, doi: 10.1063/1.4792311.

[39] J. Matas, S. Marty, M. S. Dem, and A. Cartellier, “Influence of Gas Turbulence on the Instability of an Air-Water Mixing Layer,” *Phys. Rev. Lett. 115.7*, vol. 115, no. 7, p. 074501, 2015, doi: 10.1103/PhysRevLett.115.074501.

[40] J. Yang, M. J. Anderson, P. J. Strykowski, and V. Srinivasan, “Effects of confinement on absolute

and convective instabilities for momentum-driven countercurrent shear layers," *Phys. Rev. Fluids*, vol. 6, no. 7, 2021, doi: 10.1103/PhysRevFluids.6.073901.

[41] J. Matas, A. Delon, and A. Cartellier, "Shear instability of an axisymmetric air – water coaxial jet," *J. Fluid Mech.*, vol. 843, pp. 575–600, 2018, doi: 10.1017/jfm.2018.167.